October 1985 LRP 265/85

THE ALFVEN WAVE SPECTRUM AS MEASURED ON TCA TOKAMAK

G.A. Collins, F. Hofmann, B. Joye, R. Keller,
A. Lietti, J.B. Lister, A. Pochelon

Submitted for publication to Physics of Fluids

THE ALFVEN WAVE SPECTRUM AS MEASURED ON THE TCA TOKAMAK

G.A. Collins, F. Hofmann, B. Joye, R. Keller,
A. Lietti, J.B. Lister, A. Pochelon

Centre de Recherches en Physique des Plasmas
Association Euratom - Confédération Suisse
Ecole Polytechnique Fédérale de Lausanne
21, av. des Bains - 1007 Lausanne/Switzerland

ABSTRACT

The detailed experimental data obtained on TCA concerning the antenna loading and wavefields as a function of the Alfvén Wave spectrum are presented. The plasma density, plasma current, working gas, toroidal magnetic field and frequency have all been systematically varied and the detailed results are compiled and discussed. In addition the phasing of the antenna currents has been systematically varied, thereby exciting different combinations of modes, including pure travelling waves. The conclusions which are relevant to the design of an antenna system have been stressed.

I. INTRODUCTION

In this paper we present and discuss results obtained during Alfvén Wave (AW) heating experiments on the TCA Tokamak, restricting ourselves mainly to the resistive loading of the antenna structures used, and to the observation of the waves excited. These two topics have provided a vast quantity of information of an extremely detailed nature, which has been used to confront our understanding of the fundamental processes behind the excitation of Shear Alfvén Waves in a tokamak.

TCA[1] is a small circular cross-section tokamak with the following parameters: R,a = 0.61,0.18 m; B_ϕ = 0.7-1.51 T; $I_p \leq 170$ kA; $\bar{n}_e < 10^{14}$ cm^{-3}. The polished stainless steel vacuum vessel has a rectangular cross-section, with additional space at the top and bottom to accommodate the antennae. The antennae themselves, shown in Figure 1, are in eight groups. A top and a bottom group is placed in each quadrant of the torus. Each single antenna comprises three pairs of 10 mm diameter curved stainless-steel bars, fed in parallel, and coated with 6-7 μm of titanium nitride, a medium-Z hard material with a low sputtering yield. Each antenna group floats with respect to the vacuum vessel and is fed via 35 mm and 63 mm diameter vacuum ceramic breaks, in push-pull as part of a tuned circuit. A conceptual image of the generator circuit is shown in Figure 2, and it is described in detail in Ref. 2. Unless specified, the antennae were completely unshielded either in front or to their sides.

At the start of the experiments on TCA very little detailed experimental data existed on AW excitation in a tokamak. Some experimental work had been carried out on other types of machine and has

already been extensively reviewed.[3] In addition there are now other experiments on AW heating in operation, namely PRETEXT,[4] TORTUS[5], URAGAN-III,[6] TOKAPOLE,[7] and RO-5.[8] Much of the work on these machines has been carried out using magnetic probes inside the plasma, which is not feasible on TCA with its relatively high current density (~400 A/cm^2 on axis).

The work described in the following sections is notionally independent of the rf power delivered. Nonetheless earlier results,[9] recently repeated and discussed in greater detail later in this paper, showed an increase in antenna loading at the lower powers. For this reason we have, where possible, performed most absolute measurements in a region of constant, i.e. power-independent, loading, which normally corresponds to a delivered power $P_{rf} > 60$ kW.

Although many parameters have been deliberately varied to obtain the results, we nonetheless refer to "standard conditions" for much of the work described. These correspond to B_ϕ=1.51 T, $I_p \sim 128$ kA, $q_a \sim 3.1$, deuterium as the filling gas and an antenna structure phased to excite waves with toroidal and poloidal mode numbers $n=\pm2$, $m=\pm1$ as will be more amply described in Section III. The generator frequency was 2.5 MHz unless specifically defined.

The organization of the present paper is as follows. Section II describes the excitation of Shear Alfvén Waves, defining the nature of the continua excited. Section III describes the loading spectrum obtained under fixed conditions, and the measurement techniques used. The multiple-antenna structure allows excitation of different modes, and the results of many different structures are presented and evaluated in Section IV, along with implications for the antenna

design. The nature of the Discrete Alfvén Wave (DAW) spectrum is described in Section V. The value of the plasma current changes the antenna loading and this experimental result, together with some model calculations, is presented in Section VI. In Section VII we describe experiments carried out with an antenna configuration which launches travelling waves. Section VIII describes in detail the non-constancy of the loading, already mentioned, and also describes some experiments varying the antenna-plasma spacing. Finally, in Section IX, we recall the main conclusions of the paper.

II. THE EXCITATION OF SHEAR ALFVEN WAVES

The ideas behind heating a plasma using Alfvén Waves were independently developed by Dolgopolov and Stepanov,[10] Jankovich,[11] Grossmann and Tataronis,[12] and by Hasegawa and Chen.[13,14] Since then a considerable volume of theoretical work has been published. Numerical results using a kinetic model and cylindrical geometry have been obtained by Ross et al.[15] who cite a useful bibliography. Results from ideal mhd and cold plasma theory are described by Appert et al.[16-18] We shall nonetheless attempt to describe fairly crudely the excitation of Shear Alfvén Waves (SAW) in order to understand the results which shall follow.

The SAW can be excited in an inhomogeneous plasma, if the condition $\omega=k_{\parallel}V_A$ is satisfied in the plasma, in the ideal mhd approximation. When finite ω/ω_{ci} effects are taken into consideration, a resonance surface appears when $\omega=k_{\parallel}V_A(1-\omega^2/\omega^2_{ci})^{1/2}$. In periodic cylindrical geometry the oscillating fields have the form

$e^{i(k_z z+m\theta-\omega t)}$, and the resonance frequency condition can be written as

$$\omega^2 = \frac{(n+m/q(r))^2}{R^2} \cdot \frac{B_0{}^2}{\mu_0 \rho(r)} \cdot (1-\omega^2/\omega^2{}_{ci}) \qquad (1)$$

in which n is the toroidal mode-number Rk_z and m is the poloidal mode-number rk_θ, q(r) is the local safety-factor, $\rho(r)$ is the local mass-density, B_0 is the static toroidal magnetic field, R is the major radius and ω_{ci} is the (weighted) ion-cyclotron frequency. Since Equation (1) defines a frequency which itself is a function of radius, $\omega(r)$, the excited waves form a continuous spectrum from a minimum value ω_{min} which can be on or off axis to a maximum value at the plasma edge. The continuous nature of the excitable spectrum yields the well-known property of resonant absorption that the strength of the coupling to the wave is independent of both the nature and the strength of the subsequent damping mechanisms. It is precisely this property which allows the antenna-plasma coupling, measured by the antenna loading, to be calculated accurately in the mhd limit. When kinetic and other non-ideal effects are considered, the loading remains unchanged as long as the damping of the converted wave, produced at the SAW resonance radius, is strong enough.[14]

Having established the existance and dispersion relation of the SAW continua, which can act as an energy "sink", we must now try to drive the resonance. One method is to drive the vestigial wavefield of the SAW outside the plasma column, which requires antennae external to the plasma column and parallel to the static magnetic field. The approach used on TCA[19] is to excite a fast, or compressional wave of specified toroidal and poloidal wavelengths, often referred to as the driven surface wave, which will then itself couple to the SAW reso-

nance inside the plasma column. We note in passing that we are actually describing a two-step physical process to solve one set of equations, namely the plasma response to an external modulation, but we consider the description useful. The compressional wave must now be driven by the external antennae, which for TCA are purely poloidal, but which can be usefully inclined.[20] They can therefore be considered to exert a magnetic pressure modulation at the plasma boundary, equal to $\underline{b} \cdot \underline{B}$ where $\underline{b}$ is the oscillating magnetic field and $\underline{B}$ is the static magnetic field. Orienting the antennae close to perpendicular to the static field clearly produces a larger pressure modulation at the plasma surface; the electric field component parallel to the static magnetic field is also strongly reduced.

Let us now return to the dispersion relation, Equation (1) in which both the density and the safety factor profiles play a role in determining the radius of the singularity, r_s. We rewrite the externally variable part of equation (1) defining

$$\kappa_0^2 \equiv \frac{\omega^2 \mu_0 \rho(0) R^2}{B_0^2} \cdot (1-\omega^2/\omega^2_{ci})^{-1} = \frac{(n+m/q(r_s))^2}{\rho(r_s)/\rho(0)} . \qquad (2)$$

This quantity represents $k^2_{\parallel}(0)R^2$, for all conditions.

In Figure 3 we have plotted the value of r_s/a, a being the plasma minor radius, as a function of κ_0^2 and as a function of the peak plasma density for standard parameters, assuming $n_i=n_e$, for different conditions, always with $(n,m)=(2,1)$. We have set $\alpha_n=0.7,1.0,1.5$ respectively where the electron density is given by

$$n_e(r) = n_e(0) \cdot (1-r^2/a^2)^{\alpha_n} \qquad (3)$$

and we have set $q(0)=0.8,1.0,1.2$ and $q(a)=3.2$, assuming for simplicity that the plasma current is given by

$$j(r) = j(0)\cdot(1-r^2/a^2)^{\alpha_j} \; ; \; \alpha_j = q(a)/q(0) - 1 \qquad (4)$$

For more peaked current profiles and flatter density profiles the function $r_s(n_e(0))$ is non-monotonic. This can only be the case for $n/m < (\alpha_j/\alpha_n - 1)$, and is more pronounced for lower values of n/m. To illustrate some of the available sets of continua for one fixed condition we show in Figure 4 the resonance curves for $q(0)=0.95$, $q(a)=3.2$, $\alpha_n=1.2$ and $n=1,2,3,4$, $m=0,\pm1$. Generally the lower values of $|n+m|$ lie to the outside of the plasma column. The surfaces with $n/m > 0$ move out faster as the plasma density increases compared with those with $m=0$ or $n/m < 0$.

We summarize this Section by repeating that the SAW can be driven via a compressional or surface wave and that each SAW can be resonant at all densities above a certain threshold. The value of this resonant density threshold depends on the excited wave mode-numbers n and m, as well as on the toroidal magnetic field, the major radius, the driving frequency and the average mass of the plasma ions. The exact details of the current and density profiles determine the shape of the resonance profiles.

III. THE ANTENNA LOADING SPECTRUM

A. Definition of the Excitation Structure

Since we have a modular and independently driven antenna structure, we can separately fix the phases of all eight antenna groups. Decomposing the resulting antenna "structure" yields its Fourier

components, whose strengths are defined by (i) the phasings of the antenna currents, (ii) the amplitude of the antenna currents and (iii) the shape of the antennae themselves, principally their width and length. If we write

$$j_\theta(r,\theta,\phi) = \sum_{nm} I_{nm}(r)\, e^{i(m\theta+n\phi)} \tag{5a}$$

and

$$I_{nm}(r) = \frac{1}{4\pi^2} \iint j_\theta(r,\theta,\phi) e^{-i(m\theta+n\phi)} d\theta d\phi \tag{5b}$$

then we can write the cylindrically equivalent strengths as:

$$I_{nm} = \sum_i \frac{I_i}{2\pi^2 R\, \phi_A} \left[\frac{e^{-i(n\phi-\Psi_i)}}{n}\right]_{\phi_i-\phi_A}^{\phi_i+\phi_A} \frac{\sin(m\theta_A)}{m} \tag{6}$$

where $2\phi_A$ is the full width of the antenna, in the toroidal direction, $2\theta_A$ is the full poloidal length of the antenna, ϕ_i is its toroidal position, and I_i is the oscillating current in each antenna with phase Ψ_i. The summation is performed over all powered antennae, i.e. normally eight. We ignore the feed currents to simplify the argument, assuming that the current lies on a cylindrical surface. For the case of $m=0$, we replace $\sin(m\theta_A)/m$ by θ_A.

If we restrict ourselves to relative phases of $0,\pi$, by only defining the relative signs of the oscillating currents, we obtain the strengths of the excitation structures for different components. We denote the excitation structure components with capital letters, i.e. (N,M) to differentiate them from the excited waves, denoted as usual by (n,m). In Table I we list the first non-zero mode strengths for the 6 purest as well as some other excitation structures used in this

work, calculated for the geometry of TCA, namely R=0.61 m, ϕ_A=13.3°, θ_A=45°, all currents assumed to be unity. We also tabulate the dominant mode by which we shall refer to each configuration (N,M). This calculation assumes a constant current density across a single antenna, but if we calculate the strength summing over the six bars of one antenna group we obtain a maximum difference of 6.5%, for the n=4 case. The poloidal length of the antennae considerably reduces the higher-m components. The toroidal width has little effect on the lower-n components but suppresses certain n-components, such as n=14. The very high-n components, such as n=64, which are due to the mechanical design of the antennae, are irrelevant near the low-n wave thresholds. There is every advantage, therefore, in having a wide antenna group, to lower the inductance of the antenna, thereby reducing the applied voltage for a given delivered power.

B. Measurement of the Antenna Loading

Direct measurement of the voltage, current and their relative phase is difficult, not only because of access limitations but also because of the badly known distributions of return currents. Since the reactive current is dominant there are then large uncertainties in the resisitive loading. To overcome these problems we measure the voltage V cos ωt and the current I cos $(\omega t+\phi)$ at position A-A' in Fig. 2b). The real part of the admittance at this position is given by Y = I cos ϕ/V. If the transmission line to the antenna has a transfer impedance Z when terminated with the impedance R + $i\omega$L where R = R_{loss} + R_{ant}, L = L_{ant} + L_t then we can write (see Fig. 2c)) Y = R/Z^2 since $R \ll \omega L$. To calculate the plasma antenna loading R_{ant} we must measure the circuit losses R_{loss} (typically 60-80 mΩ per antenna group) and subtract them out. Only a fraction of these losses occur in

the antenna bars themselves, the remainder being dissipated in the ringing circuit. This method is valid under the assumption that both L and R_{loss} remain constant during a tokamak discharge. Since the plasma is only weakly coupled to the antenna it is not surprising that we have never seen any evidence to the contrary. The system is calibrated by the insertion of known resistances at A-A' in Fig. 2b).

C. The Loading Spectrum under Standard Conditions

In Figure 5(a) we show an example of the loading curve obtained under the standard conditions, with (N,M)=(2,1). The data were obtained using a series of shots with different target plasma densities, and allowing the natural increase in the plasma density during the rf pulse[21] to sweep through the density as a function of time. In this way a series of 6-7 shots can be used to build up a complete loading curve. The magnitude of the loading is always defined as the average over all the active antennae.

The main features to notice are as follows. There are three major narrow resonance peaks of relatively high antenna loading, with a fairly featureless spectrum around them. The featureless part corresponds to the sum of the various continua and the peaks correspond to the Discrete Alfvén Wave[22] spectrum. We have indicated on the figure the estimated thresholds of the four continua (n,m)=(2,-1),(2,0),(2,1) and (2,2), below the higher three of which the dominant DAW's occur. The DAW spectrum is part of the ideal mhd spectrum and has been extensively studied theoretically[23-24] since its observation. The detailed measured properties of the DAW spectrum will be discussed later in Section IV. We have demonstrated that the excitation of the (2,0) and (2,2) peaks and also the relatively large amplitude of the

continuum between the (2,0) and (2,1) DAWs are due to the toroidal coupling between different cylindrically pure waves.[25]

In Figure 5b),c) the rf wavefields normalised to the antenna current and their phases are plotted as a function of density. These data were obtained with three orthogonal magnetic pick-up coils placed inside ceramic tubes at the top of the torus between two antenna groups and in the shadow of the limiter. The coils were wound with ~14-20 turns of 300-460 mm^2 each. We see a rich structure associated with the continuum thresholds and the DAWs, and the information obtained has been used to confirm the identification of the mode numbers.[26] The phases show rapid changes at the loading peaks, corresponding to the high-Q resonant behaviour of the DAW. The amplitudes show the effects of the interference between the DAW and the underlying continua, particularly at the toroidally coupled DAWs in which case the resonant amplitudes are comparable to the underlying amplitudes. There is no strong development of either the amplitude or phase of the separate components in the continuum regions, but their values change at each threshold.

It can be shown that the antenna loading, under ideal mhd restrictions and constant profiles, is only a function of κ_0^2 and ω. Furthermore, the ω-dependence is such that $R_{ant}(\omega) \sim \omega$ for κ_0^2=constant, corresponding to a fixed amount of work done by the antenna per cycle. This reduces to the phase and amplitude of the displacement of the plasma column being a function of κ_0^2 only. The frequency dependence and magnetic field dependence of the form of the loading curve were clearly and separately shown in very early experiments.[22] Figure 6 shows the strong frequency dependence along with a very weak field dependence when the same spectral condition is excited. The two curves

and their data points correspond to two points in the spectrum, with one pair of antennae active. More recent and precise experiments have shown up a measurable difference between the antenna loading obtained with hydrogen or with deuterium as the filling gas. In Figure 7 we show the loading spectrum a) in standard conditions b) at 1.16 T and c) at 1.5 T in hydrogen, as a function of $\overline{\kappa^2} = \kappa_0^2 \times \overline{n_e}/n_e(0)$. Curves 7a) and b) illustrate well the constancy of the loading in the continua as a function of $\overline{\kappa^2}$ when the magnetic field is varied, with $\langle A \rangle = 2.0$. In order to align roughly the Discrete Alfvén Waves in hydrogen (Curve 7c)) we are obliged to set $\langle A \rangle = 1.3$. This discrepancy with the value of 1.0 for pure hydrogen was previously observed;[22] the presence of carbon as the dominant impurity and a value of $\langle Z \rangle = 3.0$ yields an effective mass which can explain the discrepancy. The absolute value of $\overline{\kappa^2}$ differs by up to 15% from the calculated value. This is, however, within the limits of uncertainty of the measured values of B_0^2 and $n_e(0)/\overline{n_e}$.

To summarize, we have shown in this Section the nature of the antenna loading spectrum, and demonstrated its scaling with the important parameters frequency, magnetic field and working gas. The detailed information obtained on the wavefield amplitude and phase variations should allow a stringent test of theoretical models which can predict the wavefields.

IV. EFFECTS OF VARYING THE EXCITATION STRUCTURE

A. Full Antenna Structure

We showed in Section III.A that, by inverting some currents in the eight antenna groups, we can change the dominant modes. We now present and discuss the results obtained during such experiments, in which the plasma conditions were as standard and in which the total antenna structure was used. Figure 8 shows the loading curves obtained in all 6 configurations. From these results we make the following observations.

Comparing the curves 8a),b),c) all with M=1 and with N=2,1,4 respectively, we see immediately that there is negligible toroidal mode number mixing, possible through antenna unbalancing. Specifically, the large DAW labelled (2,1) does not appear in the (N,M)=(4,1) or (1,1) loading curves. There is a peak close to the resonant density in the (N,M)=(1,1) case, which can be separately identified as (n,m)=(3,0). The cross-coupling is estimated to be less than 2 mΩ from a DAW with 150 mΩ loading, indicating a rejection of at least 75:1. This rejection is very different from the case of ICRF launching, in which the absorption is assumed to be very local to the antenna, and in which there is only marginal interaction between several antennae in the torus. In this latter case the concept of $k_{\parallel}$ shaping is valid and the size and shape of the antenna current elements is dominant. For AW launching the concept of $k_{\parallel}$ shaping is meaningless and the only important factor is the Fourier decomposition of the antenna structure, which is a quantized "n-shaping". The high rejection ratio must be related to the absorption length being extremely long compared with the wavelength, to define correctly the Fourier components.

Considering that the DAW resonance quality factor Q is given by $1/Q=\Delta\omega/\omega=0.5\Delta n_e/n_e$, Figure 5 shows that Q ~ 35, similar to the value noted earlier on TCA.[22] The upper limit on the measurement of the rejection ratio, which should be equal to $9Q^2/16$ for the pollution of N=4 by an n=2 wave, is therefore compatible with the measured resonance width. In order to obtain these spectrally clean conditions, considerable attention had to be given to the antenna balancing, ensuring both the correct phase and the correct current in all eight antennae.

The curves 8a), b), c) also show that, with our eight antennae and in the standard conditions, the excitation structure (N,M)=(2,1) has the highest loading. The (N,M)=(4,1) structure may have a higher loading at a higher value of $\overline{\kappa^2}$, but no data are available at the higher frequency necessary. The frequency presently used is too low, for the operational range available to the tokamak, to explore N=4 thoroughly. A final remark concerning the M=1 loading curves is that the value of the loading increases considerably at the m=0 and m=1 thresholds but not at the m=-1 thresholds. The (2,0),(2,1) thresholds and the (4,-1) threshold show this behaviour well at $\overline{\kappa^2}$ = 3.0,7.0 and 7.0 respectively.

Figure 8d),e),f) are the M=0 loading curves. Comparing the (N,M)=(2,0) and (N,M)=(2,1) curves a) and d) we see that the (n,m)=(2,0) DAW is not excited by the (N,M)=(2,0) antenna structure, but is only present as the result of toroidal coupling, as argued before.[25] The (n,m)=(2,2) DAW is excited directly by the (N,M)=(2,0) antenna, which of course contains an m=2 component, shown simply by its presence and the absence of an (n,m)=(2,1) DAW. The same observations are repeated for the (n,m)=(3,0) and (1,2) DAWs, curves b) and e). Two

main conclusions can be drawn from these observations. Firstly, the m=0,2 contributions to the loading of each of the N=1,2 and 4 structures are small compared with the m=1 contribution. Secondly the contribution of the toroidally coupled m=0,m=2 waves is strong compared with their direct excitation by an M=0 excitation structure. This means that there is no real advantage in purity obtained by selecting the m components to be 1,3 etc, by having both top and bottom antennae. This will be shown again later in Section IV.B.

Let us try to see all this more qualitatively in terms of the excitation as a matrix equation given by

$$\underset{L}{(n,m)} = \underset{C}{(nm,n'm')} \times \underset{S}{(I^2 n'm')} \qquad (7)$$

Loading = Coupling x Structure

We note that the use of (n,m) to describe the waves in toroidal geometry implies that (n,m) are labels rather than mode-numbers. The (n,m) labelling is the same as the mode-number attribution in cylindrical geometry, and the identity of the surfaces can be followed as the aspect ratio is smoothly reduced from infinity to ~3.

The fact that the C(nm,n'm') ~ 0 if n≠n' has been shown by the toroidal mode purity. The C(nm,nm) are the direct excitation strengths, calculable fairly accurately in cylindrical geometry. C(nm,nm') with m≠m' are the toroidal coupling strengths. For the submatrix n=2 we can make the following observations, by inspection of Figure 8a) and d). C(2m,20) must all be small, as indicated by the lack of a directly excited (n,m)=(2,0) DAW. On the other hand C(20,21)

is large, corresponding to toroidal coupling to this DAW. Similarly C(22,21) is significant. C(22,22) is measurable, seen by the direct excitation of the (n,m)=(2,2) DAW by the (N,M)=(2,0) structure. The major contribution to the loading is the C(21,21) strength, much larger than the C(2-1,2-1) strength which is the major source of antenna loading below the (n,m)=(2,0) DAW.

As a final remark to this subsection we note that the low value of the (N,M)=(4,0) loading at low density, below the (n,m)=(4,-2) threshold ($\overline{\kappa^2} \sim 3$) sets an upper limit on the possible "non-mhd" loading, considered to be very important for unshielded antennae by some authors. This small loading, estimated as $R_{ant} \leq 5$ mΩ can be due to real loading in the (n,m)=(4,m), m<-2, continua and therefore represents an estimate of the maximum non-mhd loading at the higher powers. It cannot be excluded that electrostatic waves driven directly in the scrape-off layer could not also contribute to this loading. This is all discussed in greater detail in Section VIII.

B. Subsets of the Antenna Structure

The previous subsection IV.A dealt with the six purest configurations available with the eight antennae. By exciting subsets of these eight antennae we can excite different mixtures of Fourier components of the antenna structure. We now illustrate this with some interesting cases.

The loading curves for N=2 excitation with the four top antennae only and the four bottom antennae only are shown in Figure 9(a,b). The antenna loading per antenna is reduced from the typical case shown in Figure 5. Exciting only the top antenna, the Fourier component mix is

obviously exactly the sum of the M=1 and M=0 cases since they do not possess any common components. Equation (4) shows that the value of I_{nm} is equal to

$$I_{nm}(N=2,\text{bottom}) = I_{nm}(N=2,\text{top}) = \frac{1}{2}\left[I_{nm}(N=2,M=1) + I_{nm}(N=2,M=0)\right] \quad (8)$$

the factor of 1/2 coming from the sum over half as many antennae. The total loading is therefore equal to $[C]x[I^2_{nm}]$

$$\sum_i R_{nm} = 1/4 \sum_i R_{nm}(N=2,M=1) + 1/4 \sum_i R_{nm}(N=2,M=0) \quad (9)$$

Since we are now summing over half as many antennae, the loading per antenna is one-half of the sum of the odd- and even-configuration loadings. The top-only and bottom-only antennae should therefore give the average of the M=1 and M=0 configurations. Figure 9c) shows this average, calculated from Figure 8, and the agreement is good.

Again we find a vital difference between AWH and "local" antennae such as ICRH/LHRH/ECRH, in which no difference is generally observed between the power delivered by two sources and their sum power. We can see the reason for the AWH result more intuitively in Equation (6). The total contribution I_{nm} is an integral over the whole surface area. A current element on a helical structure has the same effect on the power delivered if it is placed at the same phase on the helix. If we superimpose two current elements and write $P=I^2R/2$ it is clear that we will obtain four times the power from twice the current. It is now clearer why we obtain four times the power per unit current if we add a second helical element far from the first, but still on an antinode!

We can now reconsider the inference drawn from Section IV.A that there is no virtue in adding both a top and a bottom antenna to define the M purity thereby rejecting the m=0,2 components, these being negligible. This point of view remains valid, but the unit antenna loading suffers by removing half of the antennae. The question therefore becomes one of purely technical considerations of the minimum reasonable unit antenna loading.

In Figure 9d) we have also shown the loading curve for the case of two opposite antennae, both top and bottom, (0-0-,π-π-) in the nomenclature of Table I. This structure has M=1 imposed and N=even, N=4 being no longer rejected. The total loading now becomes

$$\sum_i R_{nm} = 1/4 \sum_i R(N=2,M=1) + 1/4 \sum_i R(N=4,M=1) \qquad (10)$$

and again, since we are summing over only four antennae, the loading should be exactly half of the sum of the N=2,N=4 contributions. This contribution is shown as a dotted curve in the figure. The agreement is less good and the discrepancy is not understood.

Next we excite adjacent antennae with opposite phases, namely (0π--,$\pi 0$--). In Figure 9f) we show the loading in this case, compared with the average of the (N,M)=(1,1) and (2,1) loadings, R = 1/2 R(N=1,M=1) + 1/2 R(N=2,M=1) to which it should be equal. The agreement again is good.

Finally we excite two different configurations namely (000π,$\pi\pi\pi 0$) which is an M=1 configuration containing all N, and (0---,π---) which also contains all N and has M=1. These two configurations, suprisingly, have the same unit loading per antenna group, namely

1/2 R(N=1,M=1) + 1/4 R(N=2,M=1) + 1/4 R(N=4,M=1). In Figure 9h),j) we plot the loading curves of these two configurations together with the calculated combination, curve 9k); the agreement remains excellent. These configurations are interesting for heating experiments, since we require twice the current per antenna in the single antenna pair case to radiate exactly the same total power as in the full four-pair mixed antenna configuration.

We summarize these sub-sections as follows. The flexibility of the antenna system on TCA has allowed us to excite six fairly pure configurations and also to excite mixed configurations. In this way we have shown that the mixing of toroidal mode numbers is negligible; the dominant coupling is to the m=1 wave compared with m=0 or 2; toroidal coupling leading to poloidal mode mixing is an important effect; the minimum observed loading of 5 mΩ, for (N,M)=(4,0) excitation, is very small compared with the standard (N,M)=(2,1) loading; the several different combinational excitation structures have shown up the derived loading curves extremely well.

V. THE DISCRETE ALFVEN WAVE SPECTRUM

The Discrete Alfvén Waves, first observed on TCA,[22] occur only for helicity $m/n > 0$ where the signs of m and n are defined by Equation (1). Considerable theoretical work has gone into the study of the DAW, which is a Global Eigenmode of the Alfvén Wave. Its separation from and beneath the threshold is a function of the density profile, the q-profile, m and n, and the value of ω/ω_{ci}.[23,24] The DAW is the low frequency counterpart of the ion-cyclotron wave, and owes its existance, as ω/ω_{ci} tends to zero, to the presence of an equilibrium

current. The DAW spectrum has been of considerable use in investigating the spectral purity and the toroidal coupling, since it is so easily identified.

Due to the profile dependences and the value of $m \neq 0$, the resonant density of the DAW depends on the total plasma current. We have identified in Figure 10a) the m=1 DAWs from n=0-4.[27] The dashed lines represent a simple calculation of the continuum thresholds.

Figure 10b) shows the n=2,m=0,1,2 DAWs plotted as the plasma current is varied, with (N,M)=(2,1) excitation. The m=0 DAW does not occur at a fixed value of line-integrated electron density. There are two reasons for this. Firstly, the radial profile of electron density is not constant as a function of plasma current, changing the ratio $\int n_e dl/n_e(0)$. The peaking of the plasma density profile at high q(a), measured on TCA,[28] leads to a lower value of $\overline{n_e}$, as the figure shows; the resonance profile being monotonic, the minimum is on axis. Secondly, the central electron temperature is measured by Thomson scattering to be roughly linear with the plasma current over the range studied. At the lower plasma currents the degree of ionization will tend to reduce. For fully stripped ions the ratio $A/Z \sim 2.0$, equal to that of deuterium; the average ion mass is not strongly affected by the impurity content. When the ions are not fully stripped the ratio A/Z will increase, leading to a greater ratio $\rho(0)/n_e(0)$, pushing the value of the resonance density towards a lower value at lower current, as the figure shows. Quantitatively, both effects are necessary to explain the m=0 DAW resonance curve. The resonance curve for m=2 is most inclined, due to the m-dependence of the threshold condition from Equation (1). The m=1 DAW falls between the two others.

An interesting observation made using the DAW spectrum concerns the sensitivity of the resonance position to the threshold condition which itself depends on the q-profile. This sensitivity has been shown by the modulation of the resonance condition by the sawtooth activity, demonstrating a measurable variation in the q-profile during the sawtooth period.[29]

VI. THE EFFECT OF THE PLASMA CURRENT ON THE LOADING RESISTANCE

We have measured the loading at three points in the spectrum while varying the plasma current: a) below the (2,0) DAW, b) between the (2,0) and (2,1) DAWs, and c) between the (2,1) and (2,2) DAWs. Figure 11a) shows that the loading increases as a function of increasing plasma current in all three cases, with similar dependences. The general trend can be explained heuristically as follows. Changing the plasma current implies changing the current profile, as q(0) remains close to 1 over a large range of q(a), with the profile becoming more peaked as the total current decreases, equivalent to a shrinking of the current channel radius. Figure 11b) shows the peak loading of the n=2, m=0,1,2 DAWs, again as a function of the total plasma current. We have taken the loading of the DAW above the coexistant continua, multiplied by $\Delta\omega/\omega$ to approximate to the general form of an eigenmode coupling. The same general trend is seen for the dominant (n,m)=(2,1) DAW as in the case of the continua.[22,27]

We have modelled the general trend using a cylindrical model of the antenna-plasma coupling.[18,20] We compute the loading of the (n,m)=(2,1) continuum as a function of plasma current making the following simplified assumptions: q(0)=0.91, leading to I_p =

$448kA/(\alpha_j+1)$, α_j being defined by Equation (4); the density profile given by Equation (3); the antennae as in TCA with purely vertical feeds. The 1-D model should be reasonable since we choose a density just above the (n,m)=(2,1) continuum threshold, with the resonance layer close to the axis (large aspect ratio), and since the (2,1) loading is a large fraction of the total loading near the threshold as seen in Figure 5. In Figure 11a) we compare the results of the theoretical model (dashed lines) and the experiment. We have calculated the loading for three values of α_n, since the measured values of α_n range between 1 and 1.6. There is a reasonably good agreement between theory and experiment, indicating that the origin of the general trend observed is well understood, considering the limiting assumptions of the 1-D model.

An interesting observation which certainly depends on the current distribution is the effect of mhd mode-activity on the antenna loading. We measure the Mirnov activity (5-20 kHz) of the poloidal field $\tilde{B}_\theta$ at a single point using a pick-up coil in a ceramic tube in the shadow of the limiter - in fact the same coil as used for the rf wavefield measurements. Under certain conditions in ohmically heated plasmas the amplitude of $\tilde{B}_\theta$ can be extremely large, up to one per cent, normally when close to an integral value of q(a). When these oscillations occur strongly the sawtooth activity disappears, as is usual, and the soft X-ray emission profile flattens,[28] both of which we assume to be concurrent with a change in the q-profile. If the rf is applied when this happens, the antenna loading increases, which may be understood in terms of a broadening of the current profile as discussed above. There is no synchronous modulation of the loading with the Mirnov oscillation. Figure 12 shows the variation in antenna loading in the (2,0) continuum as a function of the relative amplitude

of the poloidal field oscillations. The correlation is clearly very strong. The (2,0) continuum loading is current profile dependent due to the dependence of the toroidal coupling strength on the current profile.

VII. LAUNCHING TRAVELLING WAVES

Previously in the text we have used the nomenclature (n,m)=(1,1), for example, to refer to both (+1,+1) and (-1,-1) waves which have the same helicity, and which are degenerate in ideal mhd ($\omega/\omega_{ci}=0$). Equation (4) shows that when the antenna current phases are equal to 0 or π, there is no difference between the excitation of positive or negative n-values. When we phase some antennae by $\pi/2$, for example ($0\ +\pi/2\ \pi\ -\pi/2,\ \pi\ -\pi/2\ 0\ +\pi/2$), then this is no longer true. This specific case excites n=+1 and n=-3. If we invert half of the antennae to produce ($0\ -\pi/2\ \pi\ +\pi/2,\ \pi\ +\pi/2\ 0\ -\pi/2$) then the structure excites n=-1 and n=+3. In practice this was carried out on TCA by advancing half the antennae by $\pi/4$ and retarding half the antennae by $\pi/4$, by connecting a capacitor or an inductor across the tuned circuits. The resonance conditions of the n=1 and n=3 waves are quite disparate, and n=1 waves can be excited in conditions in which the n=3,m=±1 waves are not resonant.

The results of these experiments are summarized in Figure 13. A large DAW is only strongly excited for the travelling wave n=-1, seen both on the antenna loading curve and on the wavefield signals. This preference for n=-1,m=-1 compared with n=+1,m=+1 is not predicted by mhd theory unless the terms containing ω/ω_{ci} are included.[18] The presence of the ion cyclotron effects lifts the degeneracy between the

two opposite waves of the same helicity such that the natural frequency of the m=-1 compressional surface wave lies closer to the continuum threshold.[30] The results of Figure 13 are therefore an extremely clear indication of the dominance of the m=-1 waves in the antenna loading in this region of the spectrum.

In Figure 13 there is an indication of a second DAW in the spectrum, between the first, dominant DAW and its corresponding continuum, when the wave travels in the reverse direction. This is probably the m=+1 DAW which is predicted to be much more weakly excited.[18]

We note that since both the helicity and m=-1 are specified for the dominant DAW's, this DAW always travels with its momentum anti-parallel to the plasma current, or rather parallel to the electron drift direction. The same is true of the positive helicity continua, and, of course, the opposite is true for the negative helicity continua which lie radially further out. The fact that the DAW direction was unchanged when the sign of toroidal field was inverted is seen quickly since

$$(n + m/q) \xrightarrow{\text{change sign of } B_\phi} (n+ -m/-q)$$

with both the sense of q and m changing under the transformation.

To conclude this section, we have demonstrated the ability to drive travelling waves in either direction and have also confirmed the prediction that the m=-1 compressional surface wave is dominantly excited when near to the continuum threshold. This property of the m=-1 compressional surface wave not only results in the experimentally observed preference for m=-1 DAW's, but also enables good coupling to the m=-1 resonant surfaces when they are close to the centre of the plasma.

VIII. NON-CONSTANT LOADING

A. Power Effects

The first results on TCA showed up an antenna loading which was constant as a function of power.[22] These results were obtained with stainless-steel plate antennae and with lateral shields either side of each antenna group. Later results, obtained after the removal of the lateral screens, showed a non-constant loading, increasing at lower powers.[9] In this section we present the most recent results on the non-constant loading, obtained with the present bar antennae without lateral screens.

Figure 14 shows the value of the antenna loading measured during power-scans at different positions in the continua, namely above and below the (n,m)=(2,1) DAW with (N,M)=(2,1) excitation, plotted as a function of (a) rf antenna current and (b) delivered rf power. The antenna loading decreases as the rf power increases, until it reaches a saturated value beyond which it is constant up to the highest powers delivered. No subsequent change in the high-power loading has ever been observed.

Two non-exclusive interpretations are considered to explain the non-constant loading. The first model is that the scrape-off plasma provides a sink for direct dissipation of the antenna current local to the antenna, hence the use of the term "parasitic loading". The increase in P_{rf} modifies the scrape-off plasma, measured in detail on TCA,[31] up to a certain power level at which it is effectively swept away from the antenna zone. The effect of the screens on the non-constant loading is simply understood by the reduction in the scrape-

off plasma density and the lack of a dissipative medium even at low power. The alternative model similarly describes a sweeping away of the edge-plasma as the power increases, but this then causes a reduction in the genuine "mhd" loading, i.e. in the coupling to the fast wave. The second model therefore differs in that the quantity

$$\Delta P_{rf} = P_{rf} - I^2 R_{ant} \text{ (asymptotic)}$$

is not dissipated in the scrape-off region but is actually launched into the plasma.

In Figure 14 we have also plotted the variation in the loading for the case of (N,M)=(4,0) excitation which produces the lowest antenna loading, as shown in Figure 8. The non-constant part of the (N,M)=(2,1) loading exceeds this value at low current. By its definition any local parasitic loading must be phase-incoherent and therefore identical in both cases. It is quite clear that the non-constant loading cannot only be parasitic. On the other hand since the (N,M)=(2,1) has non-constant genuine loading, the (N,M)=(4,0) case should also have some genuine non-constant loading.

We have studied the non-constant loading of the two particular configurations described in Section IV.B (Figure 9h) and j)), and plot, in Figure 14c),d) the loading against delivered power and antenna current respectively. The single pair of antennae requires twice the antenna current to deliver the same power. The loading is much more a function of the total delivered power than the individual antenna currents. This demonstrates that the variation in loading is a global phenomenon rather than a near-field phenomenon. This does not, however, totally differentiate between useful and "parasitic" loading.

In order to give an absolute upper limit of the "unwanted" power dissipated through the non-constant loading we plot in Figure 14e) the value of ΔP_{rf} as a function of the antenna current for the case (N,M)=(4,0). We find a maximum of ~10 kW of "unwanted" rf power with an antenna current of 700 A.

An additional observation considered to be possibly relevant to the non-constant loading is the self-polarisation of the antennae, which are floating with respect to the torus. Figure 15 shows the variation in the self-polarisation, or floating potential, of the antennae as a function of a) antenna current and b) delivered rf power for the same conditions as in Figure 14a) and b). We see no saturation of the self-polarisation even when the antenna loading saturates. The two cases in Figure 15c) and d), correspond to one-pair and four-pair excitation of the same mode mixture. Neither the unit antenna current nor the total power determines completely the level of self-polarisation.

To summarize, we have shown that the non-constant loading may be partly a local unwanted or parasitic effect, possibly dissipating in the edge plasma, but amounting to a maximum of 10 kW. In addition there must be a substantial part of the non-constant loading which is due to genuine "mhd" excitation, and which varies with the delivered rf power, presumably via modifications of the edge plasma.

B. Antenna Spacing Effects

The coupling between the antenna and the plasma depends on the antenna-plasma spacing, and also on the wall-antenna spacing. This is not due to the evanescence of the wave, as is the case in ICRH, as the

EM wave is barely modified crossing the scrape-off plasma at our low frequency. The antenna-plasma spacing defines the rf magnetic field, b_ϕ, at the plasma surface. Since the image current of the antenna current in the torus wall cancels the useful b_ϕ, the antenna-wall spacing is also important, and should be at least equal to the antenna-plasma spacing in which case already half of the loading is lost due to the wall, as we can very crudely write, for a narrow antenna relatively close to the plasma,

$$\frac{b_\phi}{\mu_0 I_{ant}}(\text{surface}) \sim \frac{1}{(\text{ant-plasma})} - \frac{1}{2(\text{ant-wall})+(\text{ant-plasma})} \sim \sqrt{R_{ant}}.$$

For a finite width antenna both terms fall off more slowly as a function of inceasing distance.

Two experiments were carried out. Firstly the vertical position, and secondly the horizontal position of the plasma column was varied. A sequence of shots allowed the loading to be plotted out as a function of the antenna-plasma spacing, as shown in Figure 16. These studies agree roughly with a simple calculation based on the combined antenna-plasma and antenna-wall spacings, which predicts a drop-off in the antenna loading of ~10%/cm. This modest loss is encouraging for the design of larger machines.

IX. SUMMARY AND DISCUSSION

In the experiments described in detail in this paper we have systematically varied all the important parameters relevant to the excitation of the Alfvén Wave spectrum, in order to confront our

understanding of the processes involved with the experimental data. At the crudest level we have shown that the excited spectrum can be reduced to the parameter κ_0^2, thereby aligning its main features, and also aligning, quite accurately, the normalized antenna loading $R(\omega)/\omega$. The effects of magnetic field, frequency, density, mode numbers and working gas have been clearly demonstrated. The effect of current on the dispersion relation is clearly established, and the systematic dependence of the antenna loading on the plasma current agrees well with a 1-D model.

When different excitation structures drive different modes, the antenna loading is very different due to the phase coherence of the excitation. There is only a negligible parasitic or non-mhd loading observed in the most weakly excited cases for our unshielded antennae which are almost perpendicular to the total magnetic field.

We have been able to excite different mixtures of the pure configurations and in all cases the antenna loading spectrum agrees qualitatively and quantitatively extremely well with the calculated mixture. In many of our measurements the preference of $|m|=1$ excitation is clearly shown, and in our conditions this is due to the strong excitation of the m=-1 compressional surface wave. The direct excitation of $|m|\neq 1$ components is never bigger than the toroidally coupled strengths, and is, for m=0, immeasureably small. This is extremely important for the design of future antenna systems. Finally, we have clearly demonstrated our ability to drive n=1 travelling waves with a modular antenna structure.

In all the work presented we have found no great discrepancy between our results and our understanding of the physics of the lauching of Alfvén Waves in TCA. These studies only investigate the process of excitation within the plasma. The questions of conversion and subsequent damping remain extremely challenging.

Acknowledgements

We wish to acknowledge the support of the whole TCA team during this work, and also many, many discussions with K. Appert, F. Troyon and J. Vaclavik . The continued support of both Prof. F. Troyon and Dr. A. Heym is recognized. The work described in this paper was partly supported by the Fonds National Suisse de la Recherche Scientifique.

REFERENCES

1 A.D. Cheetham, A. Heym, F. Hofmann, K. Hruska, R. Keller, A. Lietti, J.B. Lister, A. Pochelon, H. Ripper, A. Simik, and A. Tuszel, in Proceedings of the 11th Symposium on Fusion Technology (CEC, Luxembourg, 1981), Vol. I, p. 601.

2 A. Lietti, G. Bugmann, A. de Chambrier, A. Heym, F. Hofmann, B. Joye, R. Keller, J.B. Lister, A. Pochelon, A. Simik, W.C. Simm, J.-L. Toninato, and A. Tuszel, in Proceedings of the 9th Symposium on Engineering Problems of Fusion Research (IEEE, New York, 1981), Vol. I, p. 835.

3 J.L. Shohet, Comments Plasma Phys. Contr. Fusion 4, 37 (1978).

4 T.E. Evans, P.M. Valanju, J.F. Benesch, R.D. Bengtson, Y.-M. Li, S.M. Mahajan, M.E. Oakes, D.W. Ross, X.-Z. Wang, J.G. Watkins, and C.M. Surko, Phys. Rev. Lett. 53, 1743 (1984).

5 M.H. Brennan, R.C. Cross, B.L. Jessup, J.A. Lehane, and A.B. Murphy, in Proceedings of the 4th International Symposium on Heating in Toroidal Plasmas (International School of Plasma Physics, Varenna, 1984), Vol. I, p. 153.

6 O.M. Shvets, A.G. Dikij, I.A. Dikij, S.S. Kalinichenko, A.I. Lysoivan, N.I. Nazarov, T.Yu. Ranyuk, A.S. Slavnyj, K.N. Stepanov, and V.T. Tolok, idem, p. 513.

7 F.D. Witherspoon, S.C. Prager, and J.C. Sprott, Phys. Rev. Lett. 53, 1559 (1984).

8 R.A. Demirkhanov, A.G. Kirov, G.I. Astapenko, S.E. Il'inskij, Eh.M. Lomakin, V.V. Onishchenko, L.F. Ruchko, A.V. Sukachev, V.D. Medun, and N.I. Malykh, in Proceedings of the 9th International Conference on Plasma Physics and Controlled Nuclear Fusion Research, Baltimore, 1982 (I.A.E.A., Vienna, 1983) Vol. 2, p. 91.

[9] A. de Chambrier, G.A. Collins, P.-A. Duperrex, M. Grossmann, A. Heym, F. Hofmann, Ch. Hollenstein, B. Joye, R. Keller, A. Lietti, J.B. Lister, F.B. Marcus, J.-M. Moret, S. Nowak, J. O'Rourke, A. Pochelon, and W.C. Simm, in Proceedings of the 4th International Symposium on Heating in Toroidal Plasmas, (International School of Plasma Physics, Varenna, 1984), Vol. I, p. 193.

[10] V.V. Dolgopolov, and K.N. Stepanov, Nucl. Fusion 5, 276 (1965).

[11] Z. Jankovich, in Proceedings of the 6th European Conference on Controlled Fusion and Plasma Physics (Moscow, 1973) Vol. 1, p. 621.

[12] W. Grossmann and J.A. Tataronis, Z. Phys. 261, 217 (1973).

[13] A. Hasegawa and L. Chen, Phys. Rev. Lett. 32, 454 (1974); L. Chen and A. Hasegawa, Phys. Fluids 17, 1399 (1974).

[14] A. Hasegawa and L. Chen, Phys. Rev. Lett. 35, 370 (1975); Phys. Fluids 19, 1924 (1976).

[15] D.W. Ross, G.L. Chen, and S.M. Mahajan, Phys. Fluids 25, 652 (1982).

[16] B. Balet, K. Appert, and J. Vaclavik, Plasma Phys. 24, 1005 (1982).

[17] K. Appert, B. Balet, R. Gruber, F. Troyon, T. Tsunematsu, and J. Vaclavik, Nucl. Fusion 22, 903 (1982).

[18] K. Appert and J. Vaclavik, Plasma Phys. 25, 551 (1983).

[19] R. Keller, G. Bugmann, A. Cheetham, A. Heym, F. Hofmann, A. Lietti, J.B. Lister, A. Pochelon, and A. Tuszel, in Proceedings of the 4th Topical Conference on Radio Frequency Plasma Heating (Uni. of Texas, Austin, 1981), paper B2.

[20] F. Hofmann, K. Appert, and L. Villard, Nucl. Fusion 24, 1679 (1984).

[21] R. Behn, A. de Chambrier, G.A. Collins, P.-A. Duperrex, A. Heym, F. Hofmann, Ch. Hollenstein, B. Joye, R. Keller, A. Lietti, J.B. Lister, J.-M. Moret, S. Nowak, J. O'Rourke, A. Pochelon, and W.C. Simm, Plasma Phys. 26, 173 (1984).

[22] A. de Chambrier, A.D. Cheetham, A. Heym, F. Hofmann, B. Joye, R. Keller, A. Lietti, J.B. Lister, and A. Pochelon, Plasma Phys. 24, 893 (1982).

[23] K. Appert, R. Gruber, F. Troyon, and J. Vaclavik, Plasma Phys. 24, 1147 (1982).

[24] S.M. Mahajan, D.W. Ross, and G.L. Chen, Phys. Fluids 26, 2195 (1983).

[25] K. Appert, G.A. Collins, F. Hofmann, R. Keller, A. Lietti, J.B. Lister, A. Pochelon, and L. Villard, Phys. Rev. Lett. 54, 1671 (1985).

[26] A. de Chambrier, G.A. Collins, P.-A. Duperrex, Ch. Hollenstein, R. Keller, A. Lietti, J. O'Rourke, A. Pochelon, and W.C. Simm, Helv. Phys. Acta 57, 110 (1984).

[27] A. de Chambrier, A.D. Cheetham, A. Heym, F. Hofmann, B. Joye, R. Keller, A. Lietti, J.B. Lister, A. Pochelon, W.C. Simm, J.-L. Toninato, and A. Tuszel, in Proceedings of the 3rd Joint Varenna Grenoble International Symposium on Heating in Toroidal Plasmas (CEC, Brussels, 1982), Vol. I, p. 161.

[28] J.-M. Moret, W. Simm, private communication.

[29] A. de Chambrier, P.-A. Duperrex, A. Heym, F. Hofmann, B. Joye, R. Keller, A. Lietti, J.B. Lister, A. Pochelon and W.C. Simm, Phys. Lett. 92A, 279 (1982).

[30] N.F. Cramer, and I.J. Donnelly, Plasma Phys. 25, 703 (1983).

[31] A. de Chambrier, G.A. Collins, P.-A. Duperrex, A. Heym, F. Hofmann, Ch. Hollenstein, B. Joye, R. Keller, A. Lietti, J.B. Lister, F.B. Marcus, J.-M. Moret, S. Nowak, A. Pochelon, W. Simm and S. Veprek, J. Nucl. Mater. 128/129, 310 (1984).

Table I. Fourier Decompositon of the Antenna Structures.

Name	Antenna Phasings		Dominant Stengths (I_{nm}) [denoted nm=value]					
	Top	Bottom						
(2,1)	0π0π	π0π0	21=.45	23=.15	25=.09	61=.33	63=.11	65=.07
(2,0)	0π0π	0π0π	20=.50	22=.32	24= 0	60=.37	62=.23	64= 0
(1,1)	00ππ	ππ00	11=.33	13=.11	15=.07	31=.31	33=.10	35=.06
(1,0)	00ππ	00ππ	10=.37	12=.23	14= 0	30=.34	32=.22	34= 0
(4,1)	0000	ππππ	41=.40	43=.14	45=.08	81=.24	83=.08	85=.05
(4,0)	0000	0000	40=.45	42=.29	44= 0	80=.27	82=.17	84= 0
(1+2+3)	0π—	π0—	11=.16 21=.23 31=.15 51=.14 61=.16 71=.10 81=.07					
(Single)	0—	π—	11=.12 21=.12 31=.11 41=.10 51=.09 61=.08 71=.07 81=.06					
(Mixed)	0ππ	π000	11=.23 21=.23 31=.22 41=.20 51=.18 61=.16 71=.14 81=.12					

Figure Captions

1. Design of the TCA antennae: (a) vertical section; (b) horizontal section; (c) perspective.

2. (a) Schematic of the rf generator; (b) schematic of the matching circuits; (c) equivalent circuit for calculating the antenna loading.

3. Position of the resonance surface as a function of κ_0^2, calculated in 1-D with $\omega/\omega_{ci}=0$, varying the q- and density-profiles, for $(n,m)=(2,1)$.

4. Position of the resonance surfaces for different modes (n,m), $n \leq 4$, $|m| \leq 1$ calculated in 1-D with $\omega/\omega_{ci}=0$, and with $q(0)=0.9$, $\alpha_n = 1.2$. The values of $|n+m|$ are indicated for each group of curves.

5. Typical loading curve under standard conditions, the associated normalised wavefields, and their phases.

6. Measured loading of a single active antenna pair at two fixed spectral positions, varying the toroidal magnetic field and the generator frequency. The upper curve and points correspond to a density double that in the lower curve.

7. The loading curves as a function of the reduced parameter $\overline{\kappa^2}$: (a) standard conditions, 1.5 T, D_2; (b) 1.16 T, D_2; (c) 1.5 T, H_2.

8. Loading curves for the six purest antenna configurations. The DAWs are labelled as a function of $\overline{\kappa^2}$ by their (n,m) values.

9. Loading curves for: (a) top antennae only; (b) bottom antennae only; (c) calculated combination for (a,b); (d) opposite antennae only; (e) calculated combination for (d); (f) two adjacent antenna pairs; (g) calculated combination for (f); (h) 4-pair mixed configuration; (j) 1-pair; (k) calculated combination for (h,j). Plasma parameters are standard.

10. DAW dispersion relation for (a) different toroidal modes n=0 to 4, with m=1; (b) different poloidal modes m=0,1,2, with n=2.

11. Dependence of the antenna loading on the plasma current: (a) at points in the different continua shown as solid lines, with the 1-D model prediction shown as dashed lines; (b) for different DAWs.

12. The variation of the antenna loading in the (2,0) continuum in hydrogen as a function of the measured mhd activity B_θ/B_θ.

13. Measurements of the antenna loading and wavefields for travelling wave excitation in hydrogen.

14. Non-constant loading for different densities plotted versus a) antenna current and b) delivered rf power; non-constant loading for indentical mode structures using differnet antenna combinations plotted versus c) antenna current and d) delivered rf power; (e) excess rf power as a function of antenna current.

15. Self-polarisation potential of the antennae for different densities (a) as a function of the antenna current and (b) as a function of the delivered rf power; self-polarisation potential for excitation of identical mode structures using different antenna combinations, c) as a function of the antenna current and d) as a function of the delivered rf power.

16. Dependence of the variation in antenna loading as the antenna-plasma spacing was varied.

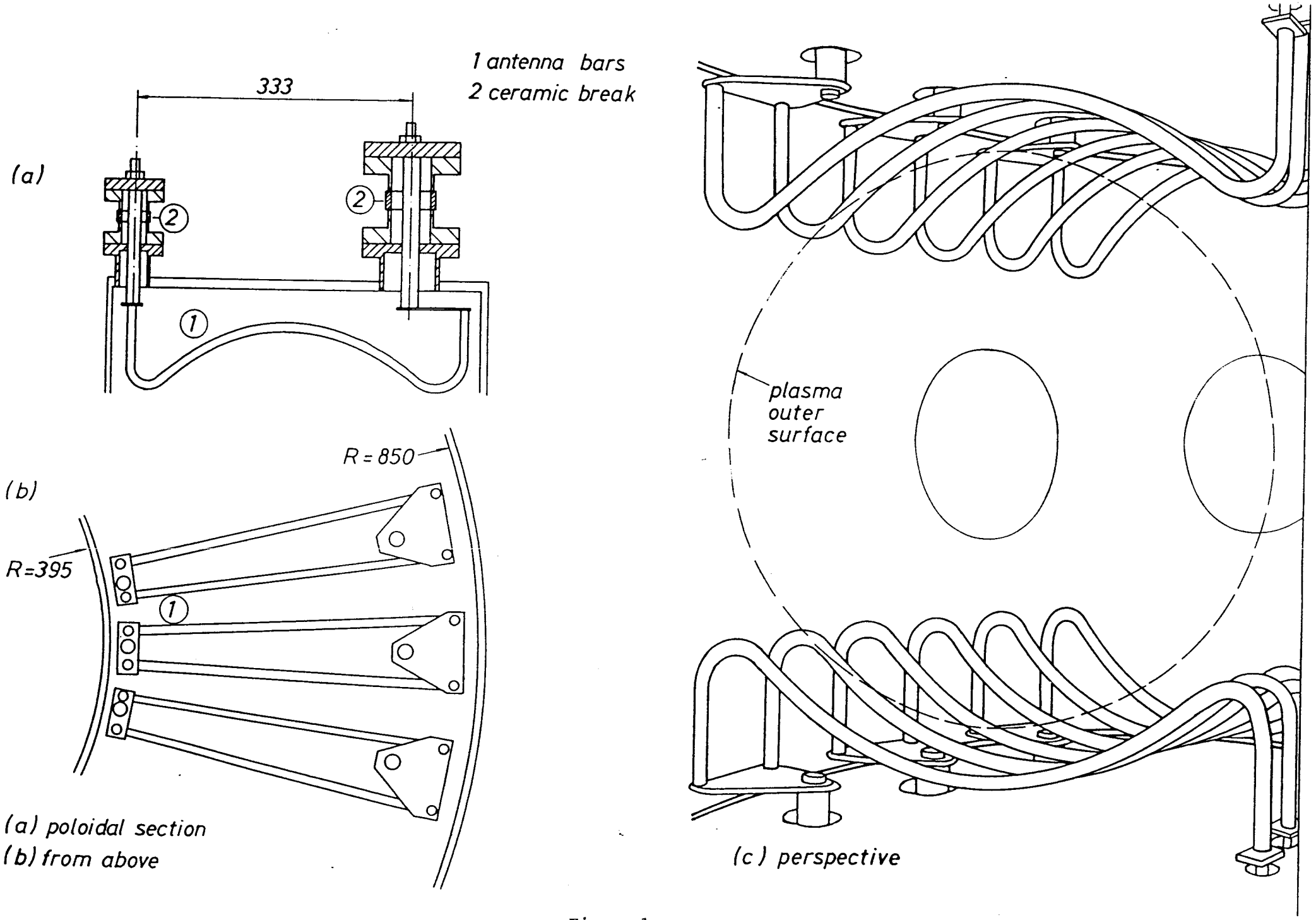
1 antenna bars
2 ceramic break
(a)
333
2
2
1
(b)
R = 850
R=395
1
(a) poloidal section
(b) from above
plasma
outer
surface
(c) perspective

Figure 1

(a)

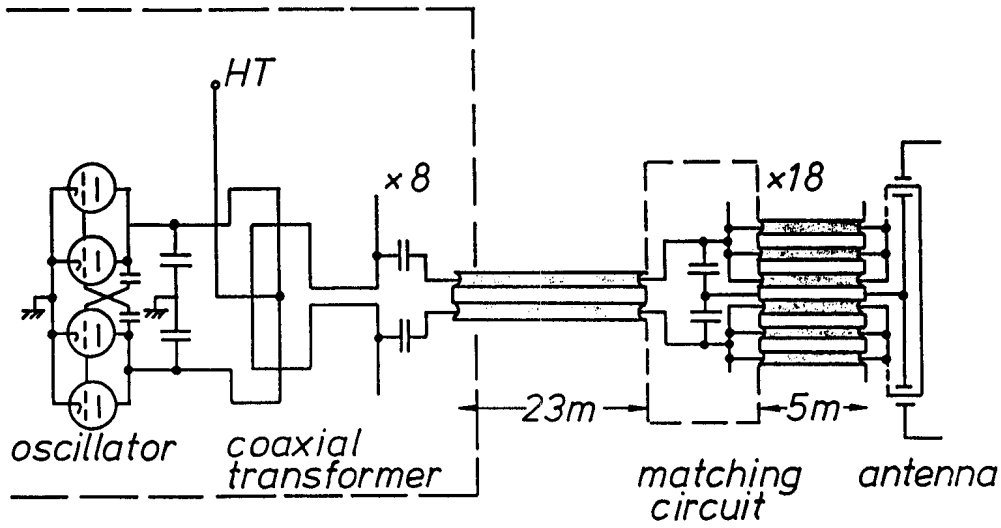
HT
×8
×18
23m
5m
oscillator
coaxial transformer
matching circuit
antenna

(b)

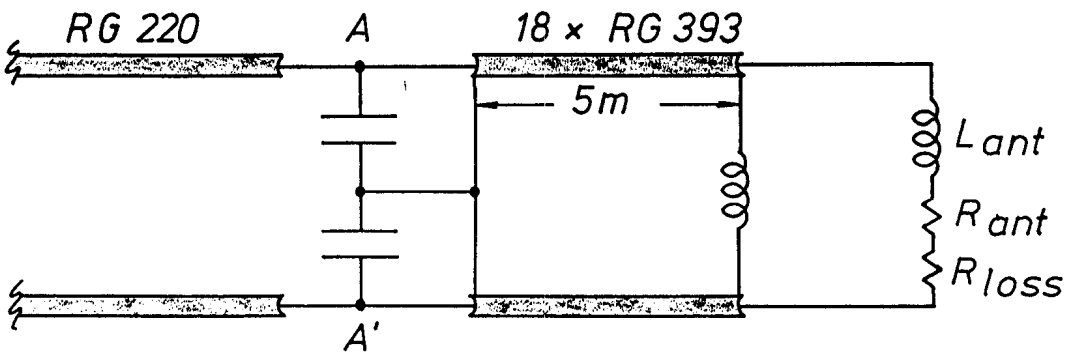
RG 220
A
18 × RG 393
5m
Lant
Rant
Rloss
A'

(c)

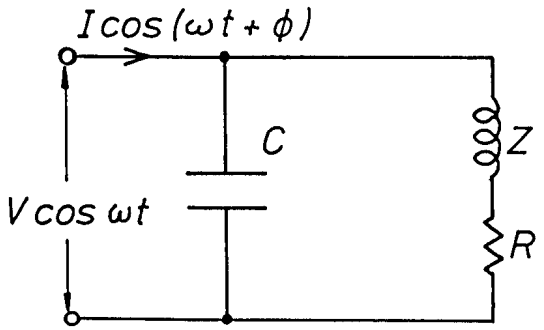
I cos (ω t + φ)
C
Z
V cos ωt
R

Figure 2

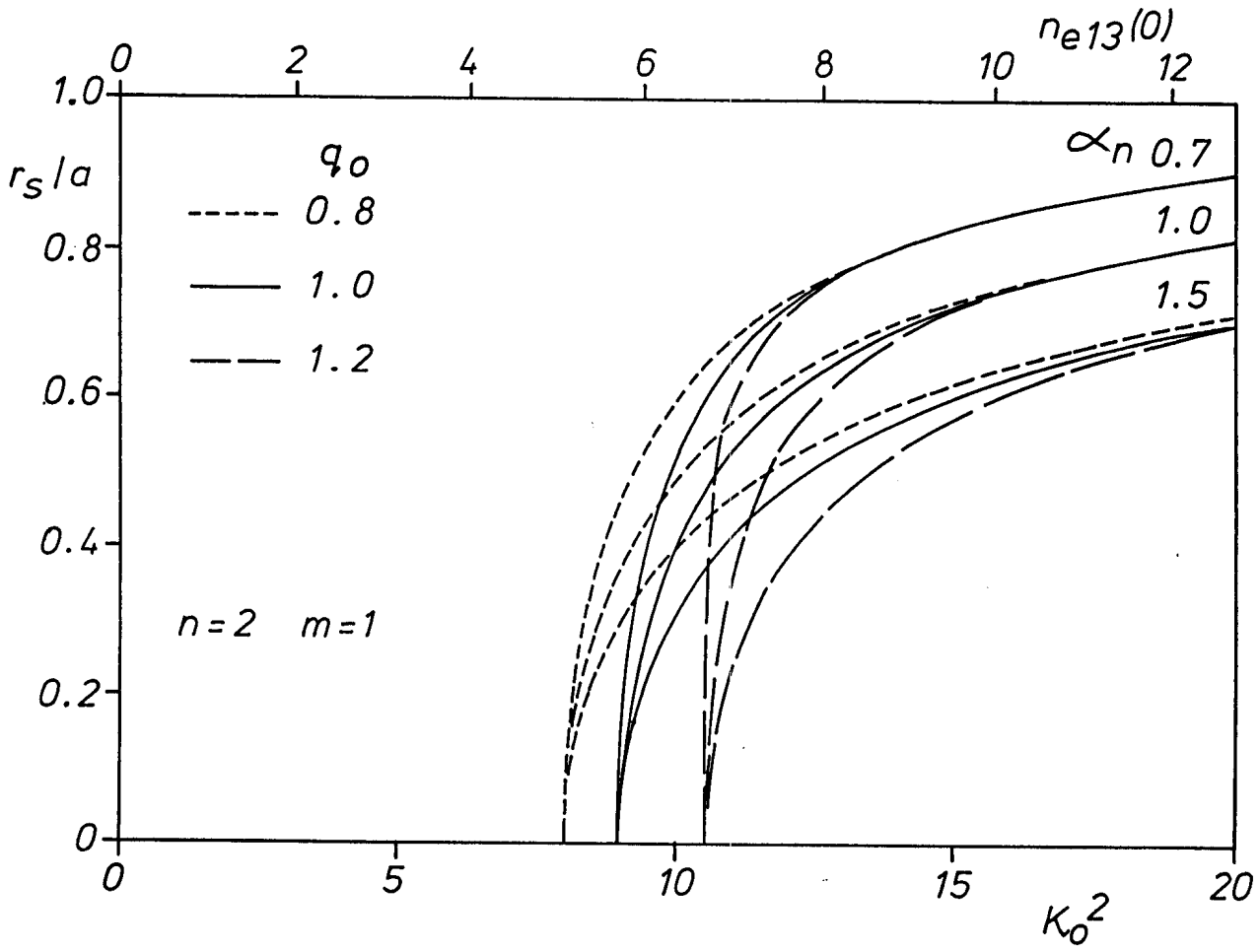
$n_{e13}(0)$
0
2
4
6
8
10
12
1.0
r_s/a
q_o
0.8
1.0
1.2
α_n 0.7
1.0
1.5
0.8
0.6
0.4
0.2
0
n=2 m=1
0
5
10
15
20
K_o^2

Figure 3

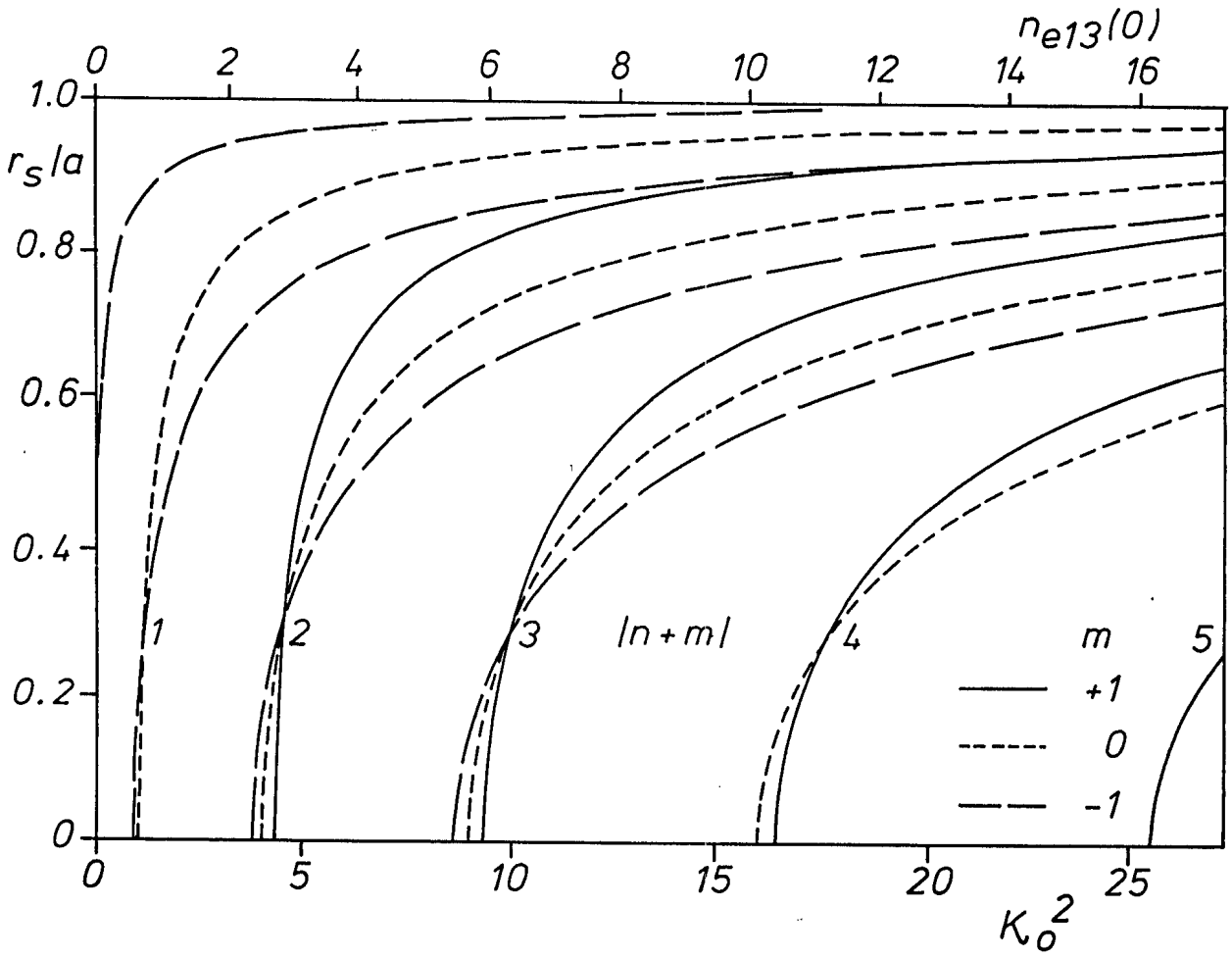
$n_{e13}(0)$
0
2
4
6
8
10
12
14
16
1.0
r_s/a
0.8
0.6
0.4
0.2
0
1
2
3
4
5
$|n+m|$
m
+1
0
-1
0
5
10
15
20
25
K_o^2

Figure 4

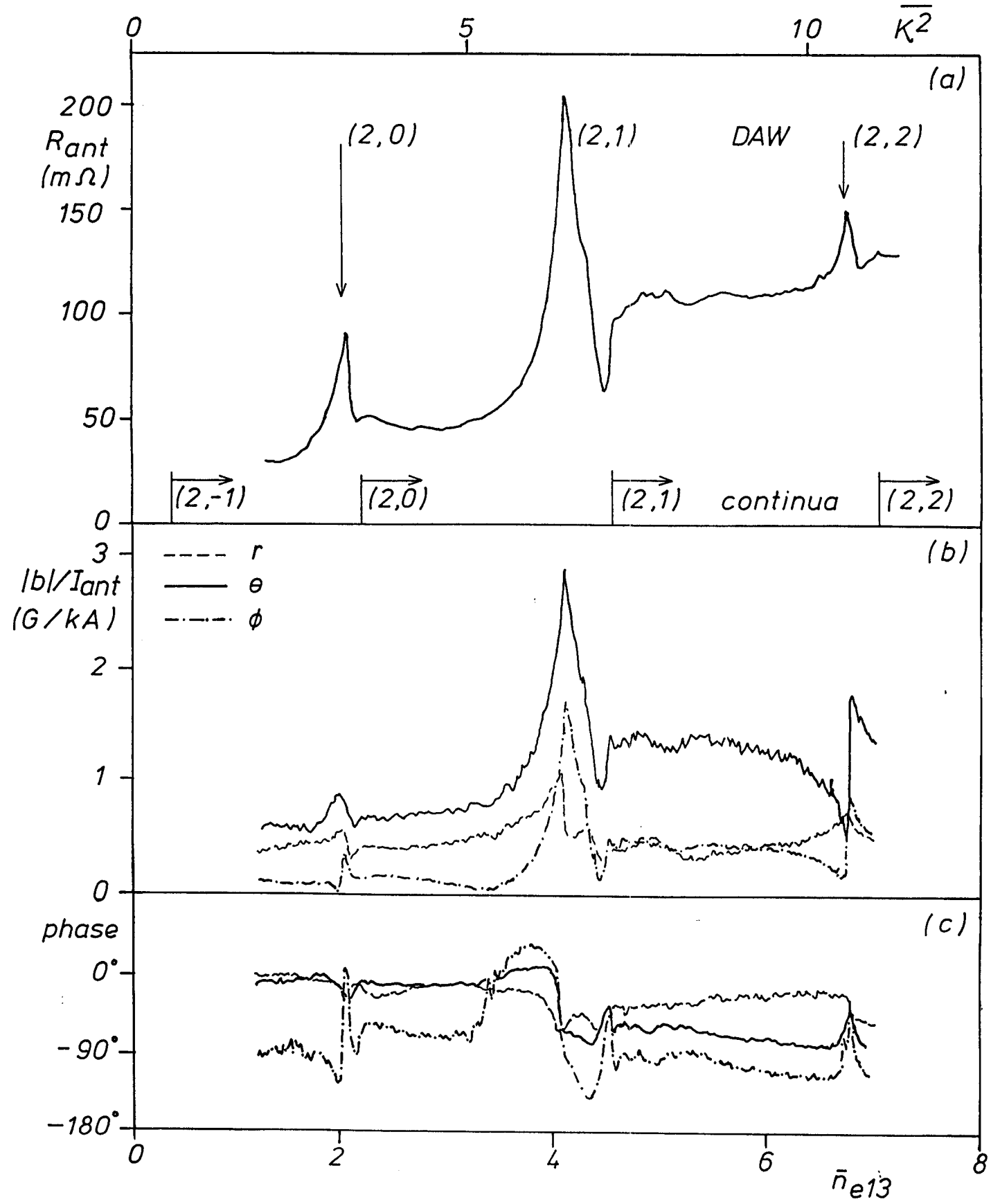
0
5
10
$\overline{K^2}$
(a)
200
R_{ant}
(mΩ)
150
100
50
0
(2,0)
(2,1)
DAW
(2,2)
(2,-1)
(2,0)
(2,1)
continua
(2,2)
3
|b|/I_{ant}
(G/kA)
2
1
0
r
θ
φ
(b)
phase
0°
-90°
-180°
(c)
0
2
4
6
8
$\bar{n}_{e13}$

Figure 5

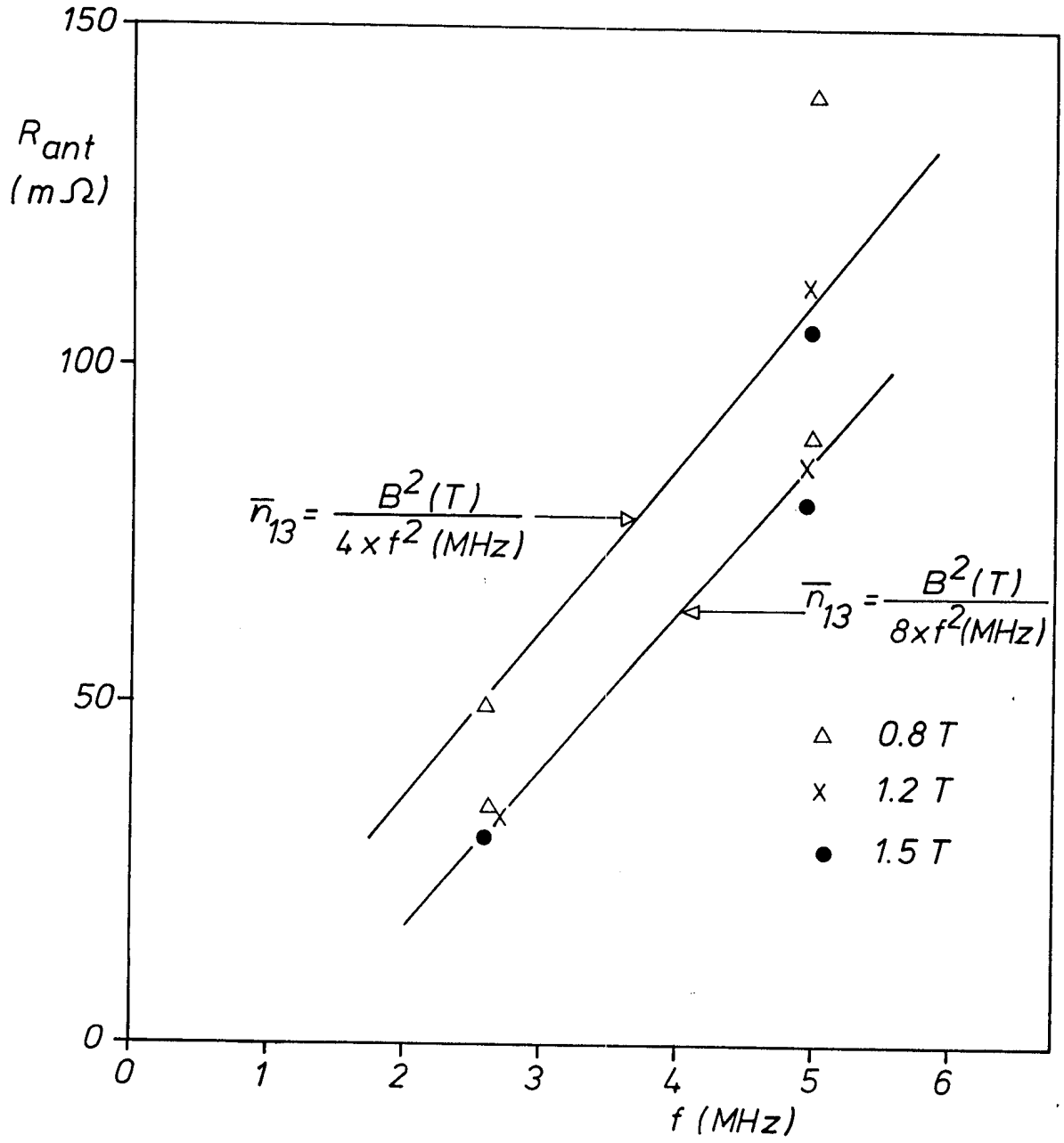
150
100
50
0
R_{ant} (mΩ)
0
1
2
3
4
5
6
f (MHz)
$\overline{n}_{13} = \frac{B^2(T)}{4 \times f^2(MHz)}$
$\overline{n}_{13} = \frac{B^2(T)}{8 \times f^2(MHz)}$
0.8 T
1.2 T
1.5 T

Figure 6

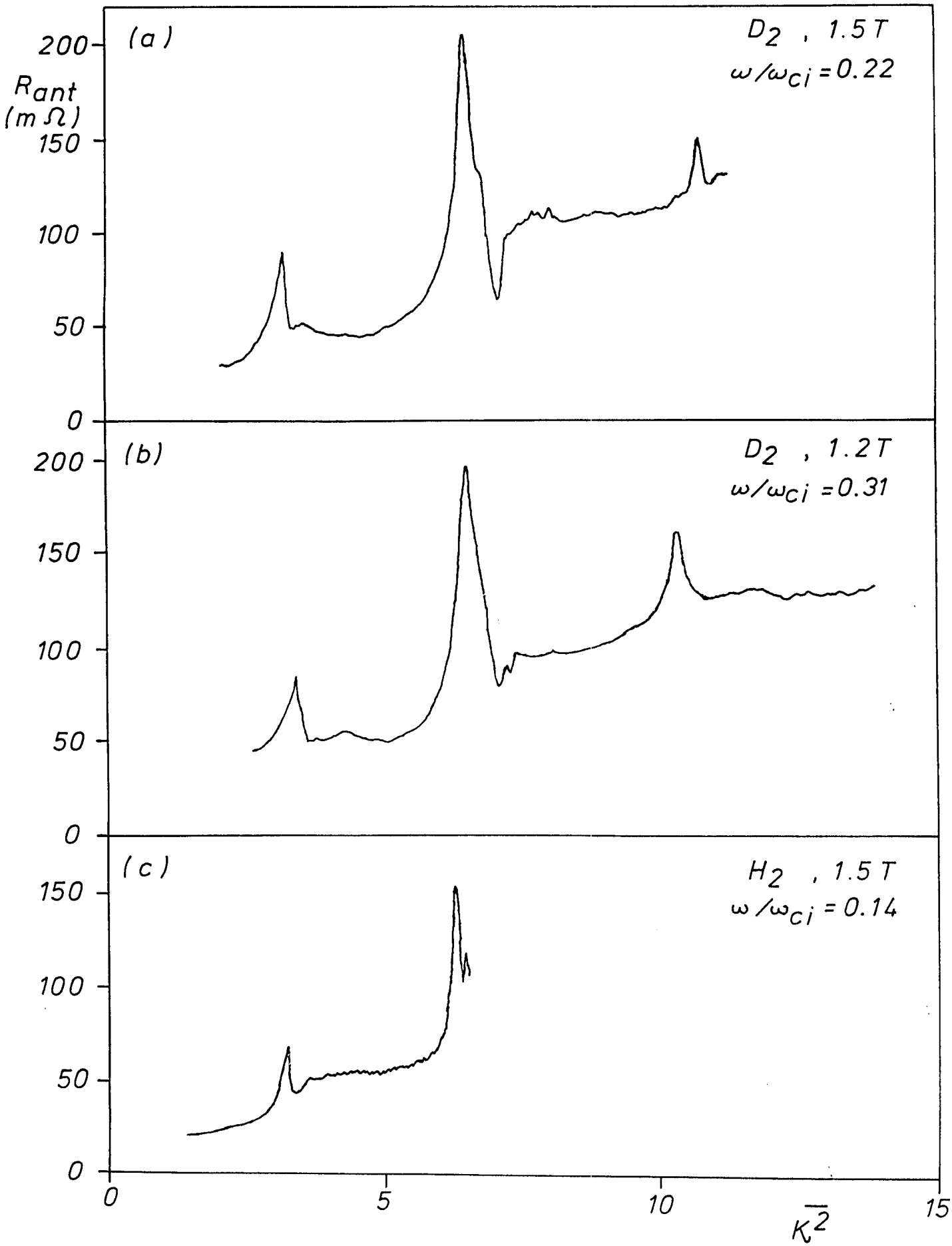
(a)
D_2 , 1.5 T
$\omega/\omega_{ci} = 0.22$
R_{ant} (m Ω)
200
150
100
50
0
(b)
D_2 , 1.2 T
$\omega/\omega_{ci} = 0.31$
200
150
100
50
0
(c)
H_2 , 1.5 T
$\omega/\omega_{ci} = 0.14$
150
100
50
0
0
5
10
15
$\overline{K^2}$

Figure 7

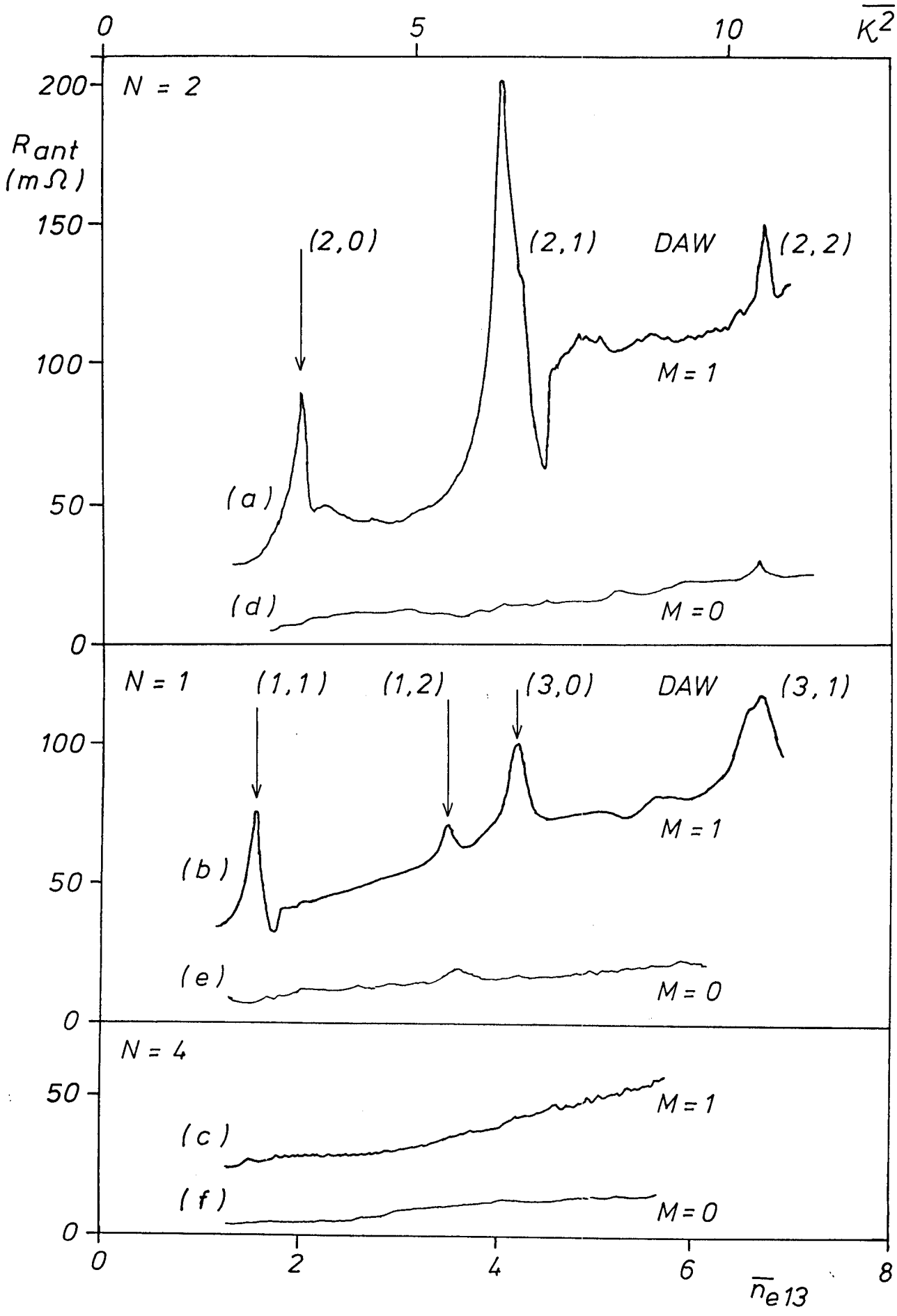
0
5
10
$\overline{K^2}$
200
N = 2
R_{ant} (mΩ)
150
(2,0)
(2,1)
DAW
(2,2)
100
M = 1
50
(a)
(d)
M = 0
0
N = 1
(1,1)
(1,2)
(3,0)
DAW
(3,1)
100
M = 1
50
(b)
(e)
M = 0
0
N = 4
50
M = 1
(c)
(f)
M = 0
0
0
2
4
6
8
$\overline{n}_{e13}$

Figure 8

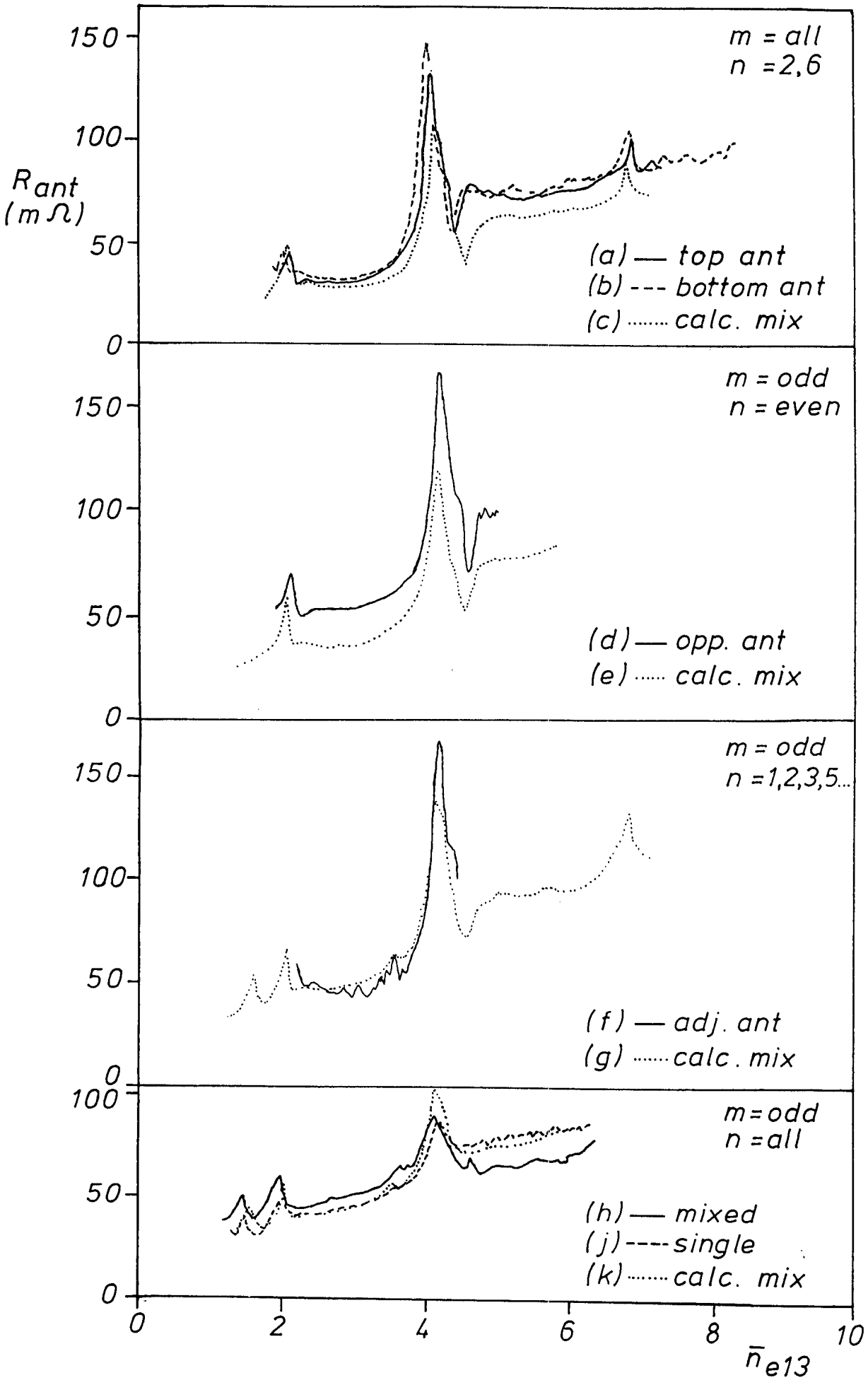
150
100
50
0
R_{ant} (mΩ)
m = all
n = 2,6
(a) — top ant
(b) --- bottom ant
(c) ..... calc. mix
m = odd
n = even
(d) — opp. ant
(e) ..... calc. mix
m = odd
n = 1,2,3,5...
(f) — adj. ant
(g) ..... calc. mix
m = odd
n = all
(h) — mixed
(j) ---- single
(k) ..... calc. mix
0
2
4
6
8
10
$\bar{n}_{e13}$

Figure 9

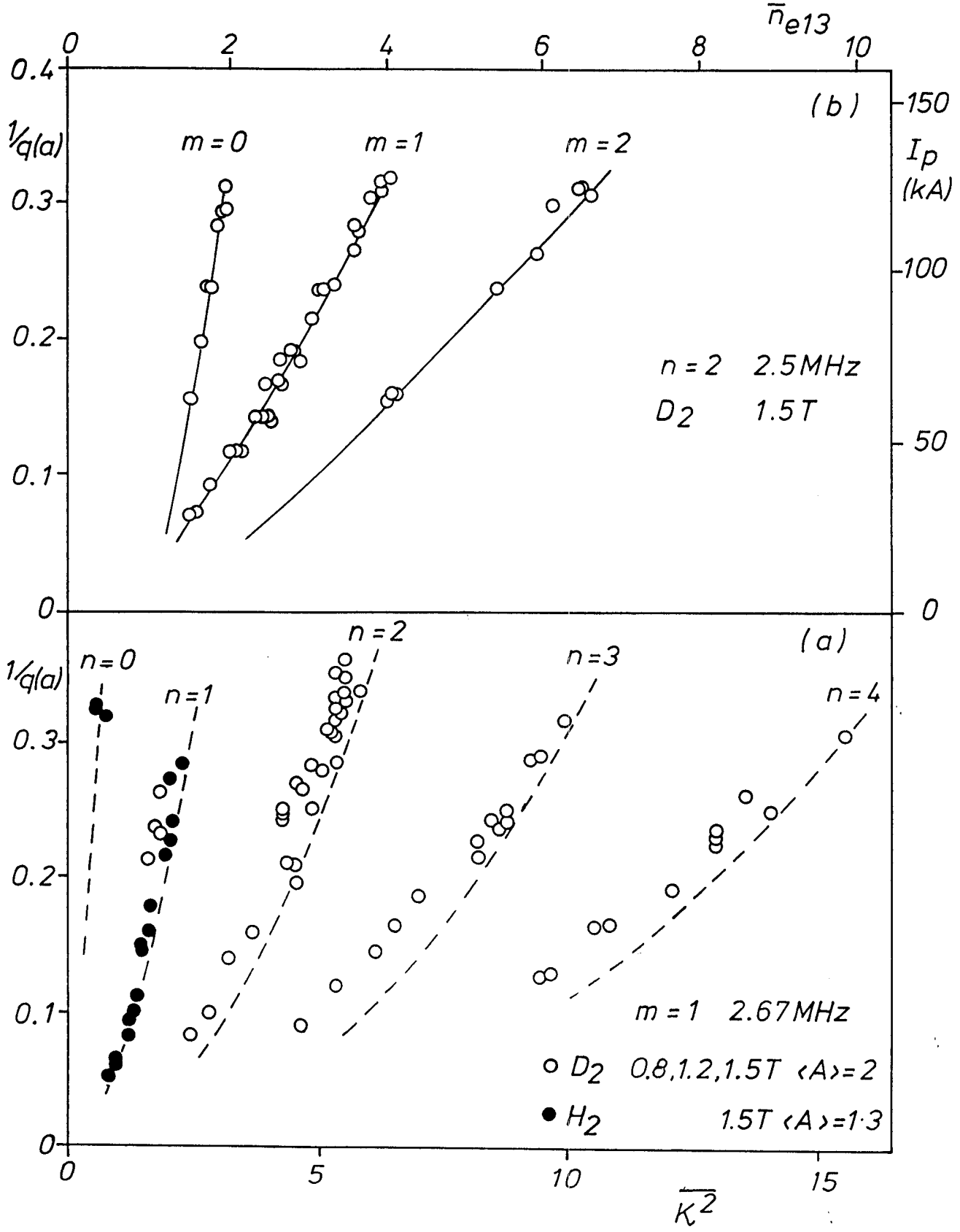
$\bar{n}_{e13}$
0
2
4
6
8
10
0.4
0.3
0.2
0.1
0
$1/q(a)$
(b)
m = 0
m = 1
m = 2
150
100
50
0
I_p
(kA)
n = 2 2.5MHz
D_2 1.5T
(a)
n = 0
n = 1
n = 2
n = 3
n = 4
m = 1 2.67MHz
D_2 0.8,1.2,1.5T ⟨A⟩=2
H_2 1.5T ⟨A⟩=1·3
5
10
15
$\overline{K^2}$

Figure 10

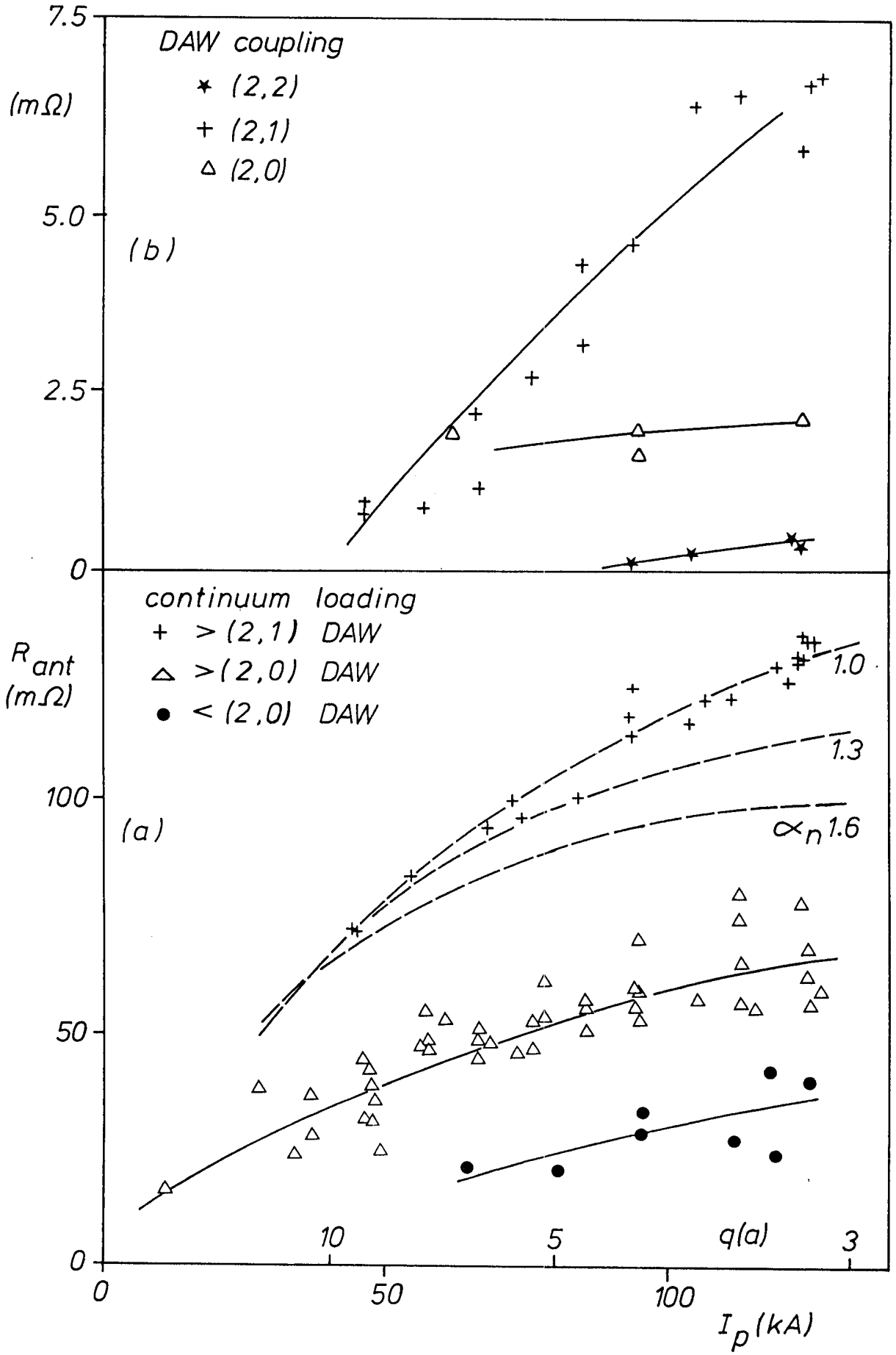
7.5
DAW coupling
(mΩ)
* (2,2)
+ (2,1)
△ (2,0)
5.0
(b)
2.5
0
continuum loading
+ > (2,1) DAW
△ > (2,0) DAW
● < (2,0) DAW
R ant (mΩ)
1.0
1.3
∝n 1.6
100
(a)
50
0
10
5
q(a)
3
0
50
100
I p (kA)

Figure 11

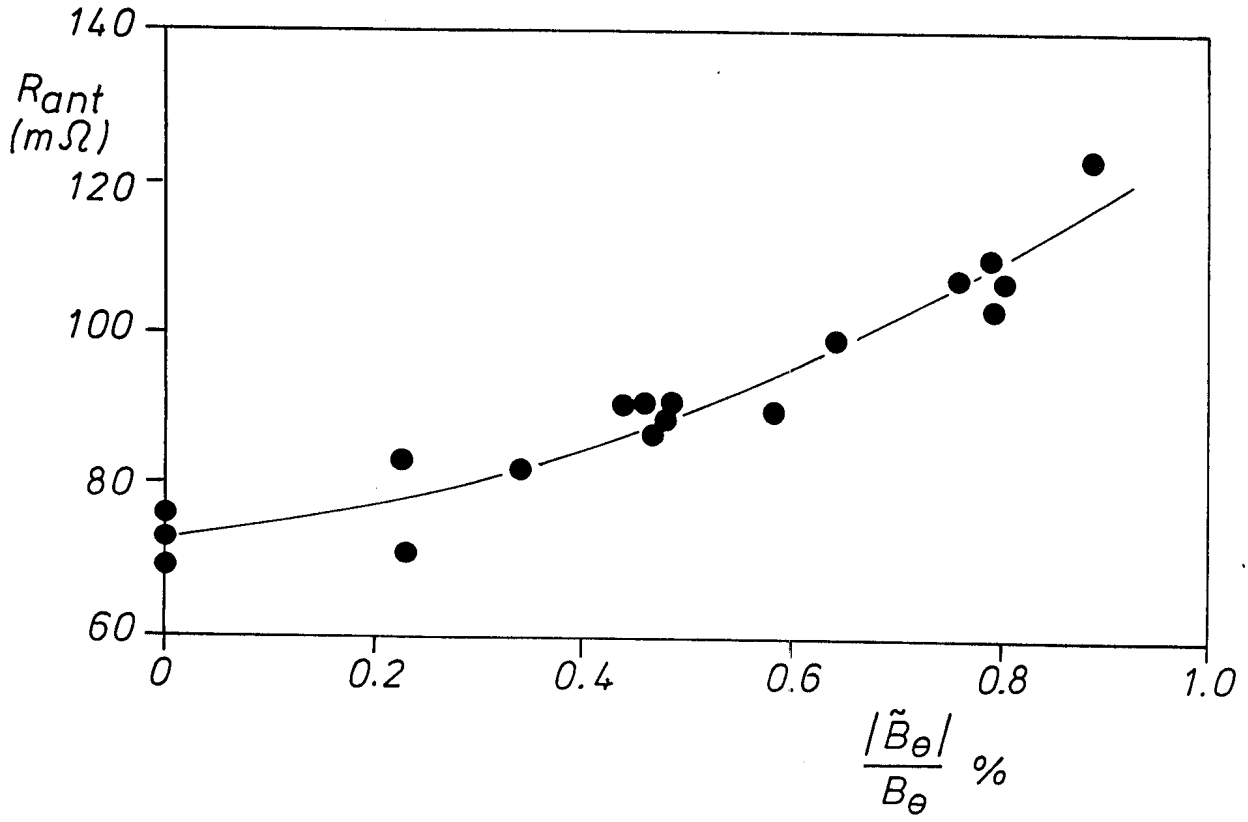
140
120
100
80
60
R_{ant} (mΩ)
0
0.2
0.4
0.6
0.8
1.0
$\frac{|\tilde{B}_\theta|}{B_\theta}$ %

Figure 12

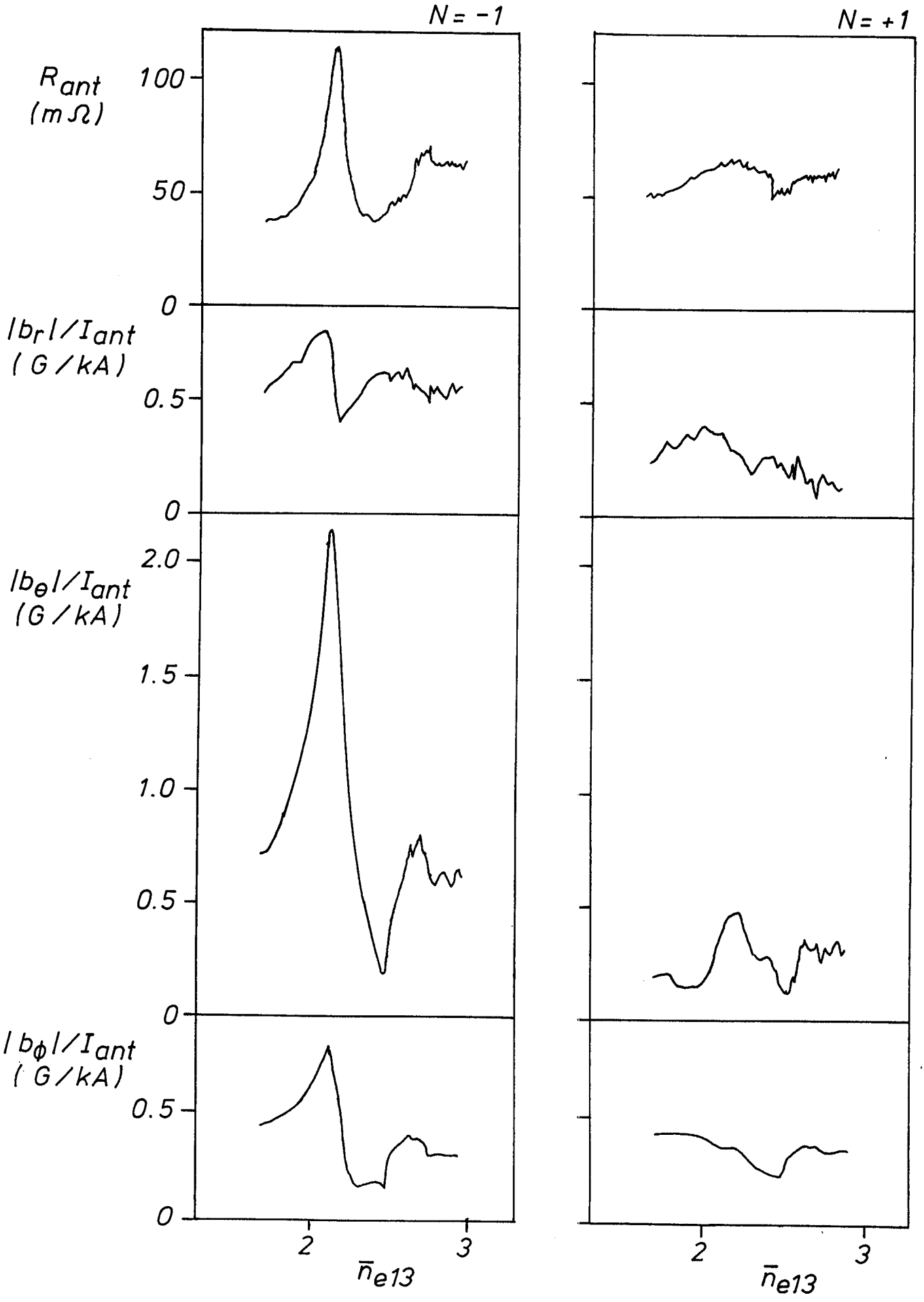
N = -1
N = +1
R_{ant} (mΩ)
100
50
0
$|b_r|/I_{ant}$ (G/kA)
0.5
0
$|b_e|/I_{ant}$ (G/kA)
2.0
1.5
1.0
0.5
0
$|b_\phi|/I_{ant}$ (G/kA)
0.5
0
2
3
$\bar{n}_{e13}$
2
3
$\bar{n}_{e13}$

Figure 13

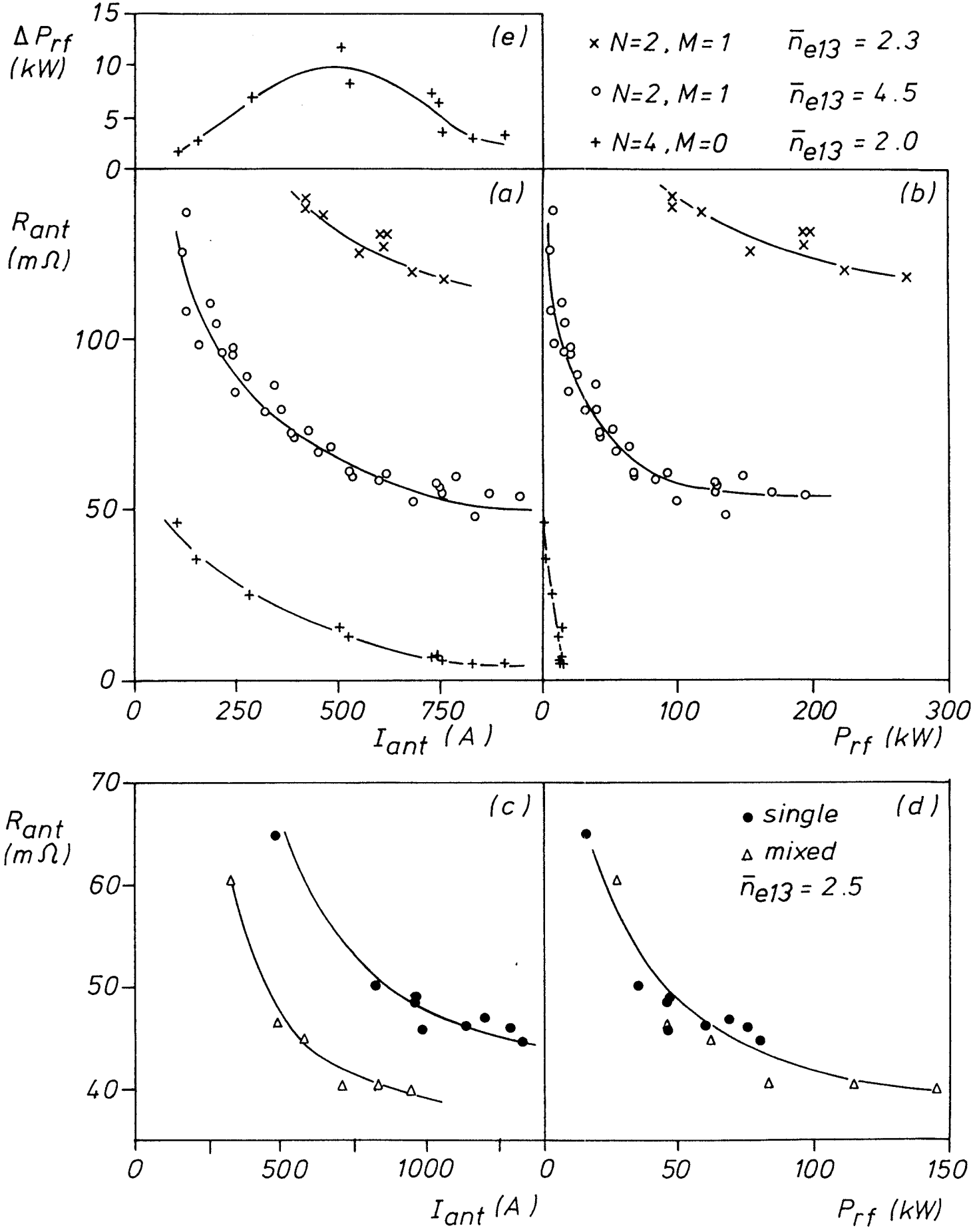
ΔPrf (kW)
(e)
× N=2, M=1 n̄e13 = 2.3
○ N=2, M=1 n̄e13 = 4.5
+ N=4, M=0 n̄e13 = 2.0
Rant (mΩ)
(a)
(b)
Iant (A)
Prf (kW)
(c)
(d)
● single
△ mixed
n̄e13 = 2.5

Figure 14

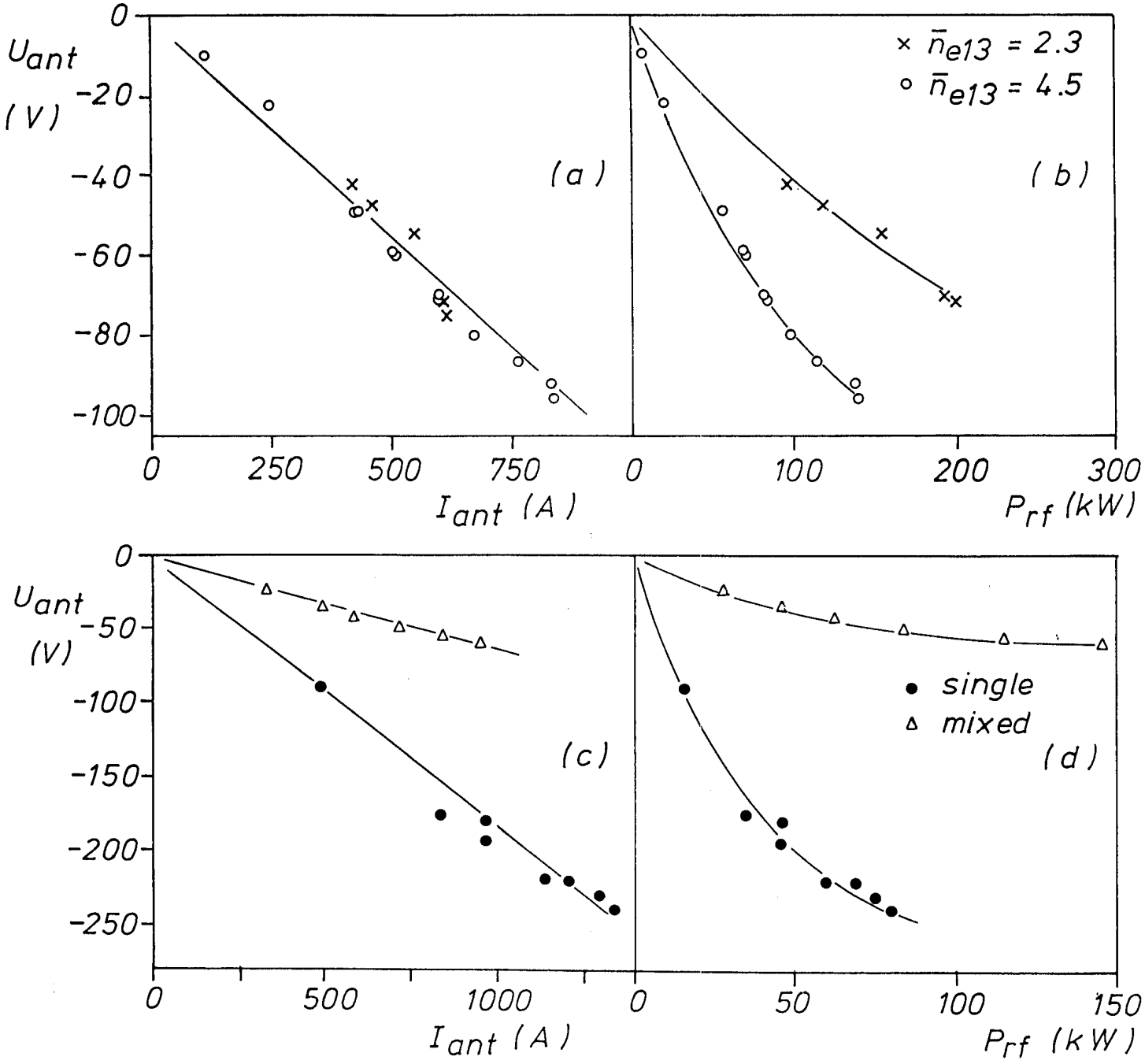
0
Uant
(V)
-20
-40
-60
-80
-100
(a)
(b)
× $\bar{n}_{e13}$ = 2.3
○ $\bar{n}_{e13}$ = 4.5
0
250
500
750
Iant (A)
0
100
200
300
Prf (kW)
0
Uant
(V)
-50
-100
-150
-200
-250
(c)
(d)
● single
△ mixed
0
500
1000
Iant (A)
0
50
100
150
Prf (kW)

Figure 15

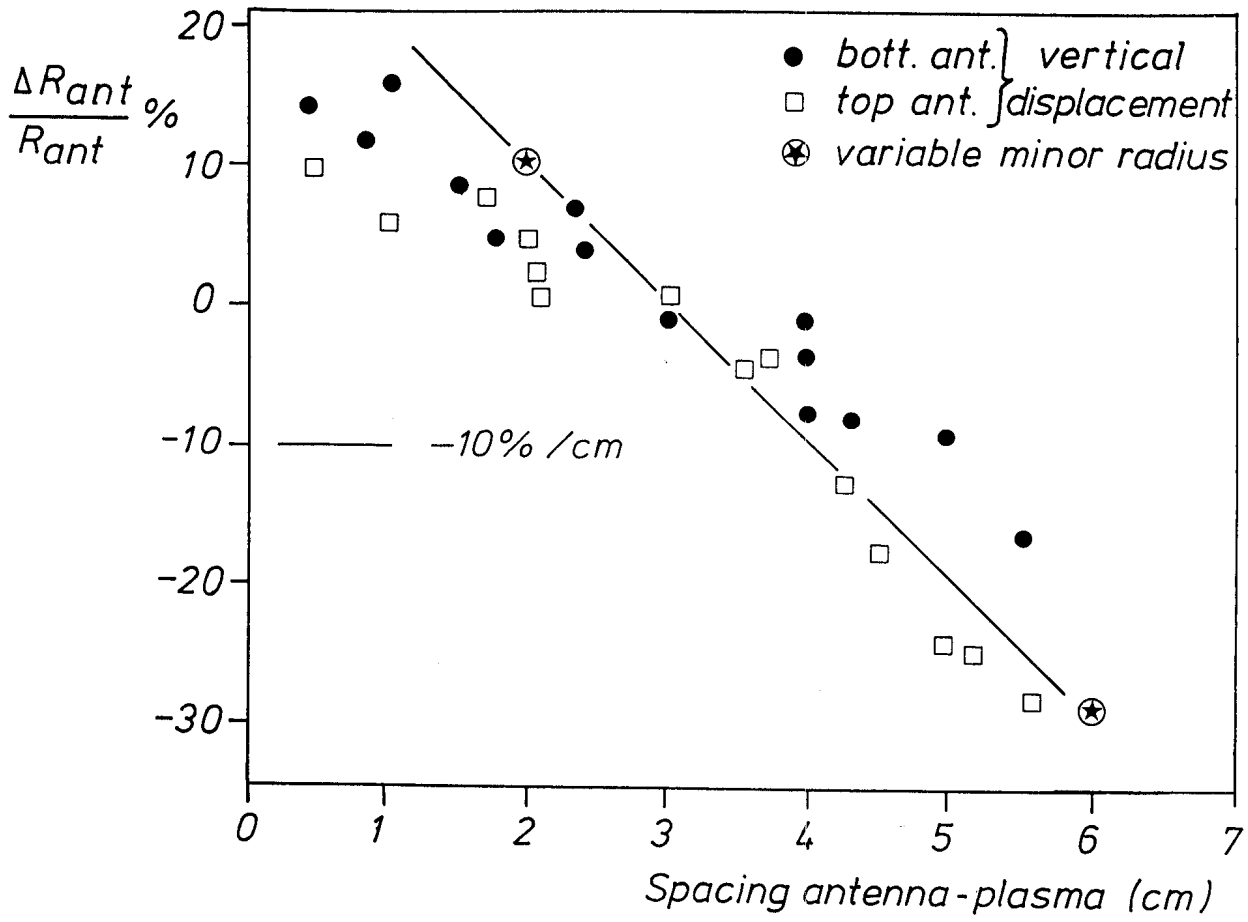
20
10
0
-10
-20
-30
$\frac{\Delta R_{ant}}{R_{ant}}$ %
bott. ant.
top ant.
vertical displacement
variable minor radius
−10% /cm
0
1
2
3
4
5
6
7
Spacing antenna-plasma (cm)

Figure 16